UNIVERSIDADE ESTADUAL DE CAMPINAS
Faculdade de Engenharia Elétrica e de Computação

Lucas Roberto Prando

Experimental Performance Comparison of Emerging Low Power Wide Area Networking Technologies for IoT

Comparação Experimental do Desempenho de Tecnologias Emergentes de Low Power Wide Area Networks para IoT

Campinas

2020

UNIVERSIDADE ESTADUAL DE CAMPINAS
Faculdade de Engenharia Elétrica e de Computação

Lucas Roberto Prando

Experimental Performance Comparison of Emerging Low Power Wide Area Networking Technologies for IoT

Comparação Experimental do Desempenho de Tecnologias Emergentes de Low Power Wide Area Networks para IoT

Dissertation presented to the School of Electrical and Computer Engineering of the University of Campinas in partial fulfillment of the requirements for the degree of Master in Electrical Engineering, in the area of Telecommunications and Telematics.

Dissertação apresentada à Faculdade de Engenharia Elétrica e de Computação da Universidade Estadual de Campinas como parte dos requisitos exigidos para a obtenção do título de Mestre em Engenharia Elétrica, na Área de Telecomunicações e Telemática.

Supervisor: Prof. Dr. Gustavo Fraidenraich

Co-orientador Dr. Eduardo Rodrigues de Lima

Este exemplar corresponde à versão final da dissertação defendida pelo aluno Lucas Roberto Prando, e orientado pelo Prof. Dr. Gustavo Fraidenraich

_____

Campinas

2020

Ficha catalográfica
Universidade Estadual de Campinas
Biblioteca da Área de Engenharia e Arquitetura
Rose Meire da Silva - CRB 8/5974

P885e

Prando, Lucas Roberto, 1994-
Experimental performance comparison of emerging low power wide area networking technologies for IoT / Lucas Roberto Prando. – Campinas, SP : [s.n.], 2020.

Orientador: Gustavo Fraidenraich.
Coorientador: Eduardo Rodrigues de Lima.
Dissertação (mestrado) – Universidade Estadual de Campinas, Faculdade de Engenharia Elétrica e de Computação.

1. Circuitos integrados. 2. Sistema de comunicação sem fio. 3. Multiplexação por divisão de frequência ortogonal. 4. Interconexão de redes (Telecomunicações). I. Fraidenraich, Gustavo, 1975-. II. Lima, Eduardo Rodrigues de. III. Universidade Estadual de Campinas. Faculdade de Engenharia Elétrica e de Computação. IV. Título.

Informações para Biblioteca Digital

Título em outro idioma: Comparação experimental do desempenho de tecnologias emergentes de low power wide area networks para IoT
Palavras-chave em inglês:
Integrated circuits
Wireless communication system
Orthogonal frequency division multiplexing
Network interconnection (Telecommunications)
Área de concentração: Telecomunicações e Telemática
Titulação: Mestre em Engenharia Elétrica
Banca examinadora:
Gustavo Fraidenraich [Orientador]
Marcos Tomio Kakitani
Cláudio Ferreira Dias
Data de defesa: 03-11-2020
Programa de Pós-Graduação: Engenharia Elétrica

Identificação e informações acadêmicas do(a) aluno(a)
- ORCID do autor: https://orcid.org/0000-0003-3958-9927
- Currículo Lattes do autor: http://lattes.cnpq.br/0531037779286798

COMISSÃO JULGADORA - DISSERTAÇÃO DE MESTRADO

Candidato: Lucas Roberto Prando RA: 211510

Data da Defesa: 03 de novembro de 2020

Título da Tese: "Experimental Performance Comparison of Emerging Low Power Wide Area Networking Technologies for IoT".
“Comparação Experimental do Desempenho de Tecnologias Emergentes de Low Power Wide Area Networks para IoT”.

Prof. Dr. Gustavo Fraidenraich (Presidente)
Prof. Dr. Marcos Tomio Kakitani
Prof. Dr. Cláudio Ferreira Dias

A ata de defesa, com as respectivas assinaturas dos membros da Comissão Julgadora, encontra-se no SIGA (Sistema de Fluxo de Dissertação/Tese) e na Secretaria de Pós-Graduação da Faculdade de Engenharia Elétrica e de Computação.

Dedico este trabalho aos meus pais Cássia e Milton, à minha namorada Taís, à minha família e a todos os amigos que me apoiaram ao longo desta jornada, iluminando com seu apoio, carinho e sorrisos cada um de meus dias.

Acknowledgements

First, I thank God for guiding me through tortuous paths. To my girlfriend, Taís Vieira, for supporting and encouraging me over the years. And I also thank my family who are my foundation and cheer for me with every step I take.

My thanks to Prof. Gustavo Fraidenraich who guided me with patience, making the dissertation days lighter.

I am grateful to Dr. Eduardo Lima for the laboratory hours in which he taught me in depth about the aspects of our research.

Special thanks to my mentor Mauro Miyashiro, the Eldorado Research Institute, the State University of Campinas and the Faculty of Electrical and Computer Engineering for the opportunity to carry out this work.

I also would like to thank my laboratory colleague, Leonardo Sulato, for all the help and instructions that he has given me, immensely contributing to the completion of the experiments. To Dr. Cláudio Dias, for the support he gave me during our work days at the Eldorado Research Institute and for the relevant tips and considerations he made about this text. To Dr. Marcos Kakitani for the suggestions made to improve this dissertation.

Finally, to all my friends who accompanied me during this journey, thank you.

"Don't waste your time looking back. You're not going that way."

(Ragnar Lothbrok)

Abstract

This dissertation presents experimental results on the evaluation of two commercial integrated circuits for IoT connectivity, using a systematic approach. One of the integrated circuits is devoted to LoRa and the other to IEEE 802.15.4g, which is the physical layer adopted by the WI-SUN Alliance. The goal behind this evaluation is to present results to support those who will make use of LoRa, IEEE802.15.4g/Wi-SUN, or other types of connectivity to fairly compare the technologies. The results show that there are differences between datasheet values and the measures collected during the experiments. There are several reasons for this divergence, such as the experimental setup, equipment calibration, transmitted packet length, and test specifications. This highlights the importance of a systematical approach when comparing technologies.

Keywords:LoRa; IEEE 802.15.4g; OFDM; O-QPSK; GFSK; Direct Spread Spectrum; Chirp Spread Spectrum; IoT; LPWAN; AWGN; Multipath.

Resumo

Esta dissertação apresenta resultados experimentais para a avaliação de dois circuitos integrados para conectividade IoT, usando uma abordagem sistemática. Um dos circuitos é dedicado a LoRa, enquanto o outro utiliza o padrão IEEE 802.15.4g adotado pela Wi-SUN Alliance. O objetivo desta avaliação é apresentar resultados que possam ajudar todos que pretendem utilizar LoRa, IEEE 802.15.4g/Wi-SUN ou outras opções de conectividade, facilitando a comparação entre essas tecnologias de forma justa e coerente. Os resultados mostram que existem diferenças entre os valores apresentados nos datasheet e os valores medidos durante os experimentos. Existem várias razões que justificam essas divergências, como a configuração dos experimentos, calibração dos equipamentos, o tamanho dos pacotes transmitidos e até as especificações dos testes. Esse resultado reforça a importância de uma abordagem sistemática para a comparação entre tecnologias.

Palavras chaves: LoRa; IEEE 802.15.4g; OFDM; O-QPSK; GFSK; Direct Spread Spectrum; Chirp Spread Spectrum; IoT; LPWAN; AWGN; Multipercurso.

List of Figures

List of Tables

List of Abbreviations

Abbreviation	**Connotation**
IOT	Internet of Things
AWGN	Additive White Gaussian Noise
SNR	Signal-to-Noise Ratio
LOS	Line-of-Sight
N-LOS	Not in Line-of-Sight
FSK	Frequency-shift Keying
GFSK	Gaussian Frequency-shift Keying
O-QPSK	Offset Phase-shift Keying
CSS	Chirp Spread Spectrum
OFDM	Orthogonal Frequency-division Multiplexing
SUI	Stanford University Interim
BW	Bandwidth
CR	Coding Rate
SF	Spreading Factor
MCS	Modulation Coding Scheme
PER	Packet Error Rate
BER	Bit Error Rate
FAN	Field Area Networks
PLCP	Physical Layer Convergence Procedure
PPDU	PLCP Protocol Data Unit
PSDU	PLCP Service Data Unit

List of Symbols

Symbol	Connotation
$\mathbb{R}$	Real number
$\mathcal{N}(\mu, \sigma)$	Normal distribution of mean μ and standard deviation σ.
$\mathcal{U}[a, b]$	Uniform distribution between a and b.
$\mathcal{R}(\sigma_r)$	Rayleigh distribution with scale parameter σ_r
$a * b$	Correlation between a and b
FFT$[\cdot]$	Fast Fourier transform of a vector
det$[\cdot]$	Determinant
$(\cdot)^H$	Conjugate transpose
Cov$[\cdot]$	Covariance operator
$\|\cdot\|$	Frobenius norm of a matrix
$\mathbb{E}[\cdot]$	Expectation
r_e	Effective radius of the earth
c	Speed of light
$A(x_A, y_A)$	Range and elevation coordinates of A on the Cartesian plane
Δ_x	Space between range samples
$f(x)$	Elevation terrain function
$f'(x)$	First derivative of terrain function
h_R	Radar hight above ground level
h_T	Target hight above sea level
v_n	Slope at the n-th terrain sample
$\psi_{in}(x)$	Incident grazing angle function
$\psi_{re}(x)$	Reflected grazing angle function
$\boldsymbol{\varepsilon}_n$	Angular error vector. Sampled version of $\varepsilon(x)$
$\boldsymbol{\omega}_n$	Inclination angle vector of the tangent line to the terrain. Sampled version of $\omega(x)$
$\boldsymbol{\gamma}_n$	Inclination angle vector of the incident ray. Sampled version of $\gamma(x)$
$\boldsymbol{\beta}_n$	Inclination angle vector of the reflected ray. Sampled version of $\beta(x)$
$\overline{\mathrm{AB}}$	Line segment that joins A and B points
d_{AB}	distance of the segment $\overline{\mathrm{AB}}$
$\boldsymbol{x_G}$	Range coordinate vector of the specular reflection points
χ	Signal-to-noise ratio of the target variable
$\hat{\chi}$	Signal-to-noise ratio of the target variable in multipath
P_t	Transmission power of the radar
G_t, G_r	Maximum gains of the transmitting and receiving antenna

List of Symbols (cont.)

Abbreviation	**Connotation**
λ	Wavelength
σ_0	Radar cross section
R	Slant range of the target
K	Boltzmann constant
T_0	Standard temperature
L_s	System loss
N_f	Noise figure
B	Receiver bandwidth
F	One way voltage multipath factor
W	Two way power multipath factor
ρ_z	Reflection coefficient of z-th reflection
ϱ	Reflection coefficient through k reflections
α_z	Phase difference of z-th reflection
$\emptyset$	Phase difference through k reflections
SW0	Swerling 0 target model
SW1	Swerling 1 target model
$f_0(x)$	Probability distribution function of x for Swerling 0
$f_1(x)$	Probability distribution function of x for Swerling 1
$\tilde{T}$	Threshold level
P_{FA}	Probability of false alarm
P_{D_0}	Probability of detection for Swerling 0
P_{D_1}	Probability of detection for Swerling 1
H_o	Sign function
θ_s	Synthetic aperture
ω	Angular velocity of ArcSAR
d	Distance from the radar center to the distributed target
r	Radius of the radar
t_k	k-th PRI
Δ_ϕ	Phase variation
f_d	Doppler frequency

List of Symbols (cont.)

Abbreviation	**Connotation**
$R_{k,i}$	Slant range vector of i-th scatterer
$s_{k,i}$	Received signal vector of i-th scatterer
$\eta_{k,i}$	Noise signal vector of i-th scatterer
$\mathrm{P}_{k,i}$	Received power vector of i-th scatterer
z_k	Composite received signal vector of a distributed target
$\bar{z}_{k,\bar{v}_{x_j}}$	Composite received signal vector of a distributed target of a j-th velocity
$\bar{\boldsymbol{v}}_{\boldsymbol{x}}, \bar{\boldsymbol{v}}_{\boldsymbol{y}}$	Possible velocity vector of the distributed target
$\hat{v}_x, \hat{v}_y$	Estimated mean velocity components of the distributed target
v_x, v_y	Mean velocity components of the distributed target
$v_{\max}$	Maximum unambiguous velocity
$\mu_{\hat{v}_x}$	Mean of the velocity estimate
$\sigma_{\hat{v}_x}$	Standard deviation of the velocity estimate
$\beta_{\tilde{\rho}}$	Phase-shift of the correlation coefficients
$\wp_\rho$	Correlation coefficients
$\mathbf{z}$	Received signal random variable vector of a distributed target
$\boldsymbol{\Sigma}$	Covariance matrix
N	number of scanning cylcles of ArcSAR
$L(\boldsymbol{\Sigma})$	Log-likelihood function
$l(\cdot)$	Likelihood function
$\boldsymbol{\Sigma}_{\mathrm{DT}}$	Sample covariance

List of Publications

- L.R. Prando, E. de Lima, L. S. Moraes, M. Hamerschmidt, G. Fraidenraich, "Experimental Performance Comparison of Emerging Low Power Wide Area Networking (LPWAN) Technologies for IoT", *IEEE 5th World Forum on Internet of Things - WF-IoT*, pp.905-908, Limerick, Ireland, Apr.2019.

- L.R. Prando, E. de Lima, L. S. Moraes, M. Hamerschmidt, C. F. Dias, G. Fraidenraich, "Packet Error Rate Measurements in Low Power Wide Area Networking Technologies for IoT", *2019 International Conference on Sensing and Instrumentation in IoT Era (ISSI) - ISSI'2019*, Lisbon, Portugal, Aug.2019.

Contents

1 Introduction

At the moment there are a number of Low Power Wide Area Networks (LPWANs) technologies candidates to provide IoT-like connectivity for applications, such as wireless sensor/actuator networks, advanced infrastructure for smart metering, public lighting, and smart cities. The main ones are: LoRa [6], Wi-SUN [7], SIGFOX [8], RPMA [9], Weightless [10], DASH-7 [11], INGENU [12] and NBIoT [13]. Each one of them has its pros and cons, regarding security, coverage, performance in non-line of sight conditions, network topology, business model, implementation/deployment/operation complexity, the data rate for up and downlink costs, and other aspects. In spite of being of paramount importance when defining a connectivity technology for IoT, those aspects will not be explored extensively in this work due to lack of space and because they are out of the scope of this work, which is oriented to Physical Layer (PHY) evaluations.

Among those technologies, the most promising ones, and which can be used in ISM (Industrial, Scientific, and Medical) and other free-use frequency bands, are LoRa and Wi-SUN. LoRa is widely known due to its very long-range attribute, especially in line of sight conditions. The long-range is achieved employing the processing gain provided by the Chirp Spread Spectrum (CSS), which uses more bandwidth than the minimum necessary to transmit the signal. A drawback is the limitation of the data rate to values lower than 40 kbps when using CSS. Nevertheless, LoRa has a GFSK mode, which also can achieve long-range communication and can be used for a 50 kbps data rate, although this is not the flagship of Semtech's LoRa chips.

The WI-SUN Alliance incentives and supports implementation and deployment of Interoperable wireless Smart Utility Networks, by adopting open industry standards as defined by international and regional standards development organizations; providing input to the standards process; and establishing conformance and interoperability certification programs. The Physical Layer adopted by WI-SUN FAN (Field Area Network) profile is IEEE 802.15.4g [3], which is an amendment to the IEEE 802.15.4 standard [14] targeting the special communications needs of Smart Utility Networks (SUNs). SUNs play a key role in the context of smart grids: they enable multiple applications to operate over shared network resources, support two-way communications among measurement and control devices of a utility system, and frequently cover widespread areas with a large number of outdoor devices. While IEEE 802.15.4 is devoted to Low-Rate (LR) Wireless Personal Area Networks (WPAN), which are used to convey information over relatively short distances with little to no infrastructure and deliver data rates up to 250 kbps,

the IEEE 802.15.4g amendment is designed to achieve data rates from 6.25 kbps to 800 kbps [15] and to work in several frequency bands, from 169 MHz to 2.4 GHz. The IEEE 802.15.4g has three possible modulations: GFSK (for good transmit power efficiency due to the constant envelope of the transmit signal), O-QPSK (uses Direct Spread Spectrum and share the characteristics of the O-QPSK PHY defined in the IEEE 802.15.4 standard released in 2011) and OFDM (for providing higher data rates at higher spectral efficiency). Currently, the FAN profile of Wi-SUN adopts the GFSK modulation only, but the use of other modulations is foreseen.

There are many papers and publications on the subject of LoRa's and Wi-SUN's (802.15.4g) performance. Most of them bring the theoretical discussion, displaying theoretical and simulation results discussing how the created mathematical models should be a good representation of the modulations since they have results close to the expected. These analyses and models can then be used to advance the understanding of the technologies and further test new approaches and algorithms to improve them.

About LoRa, it is also common to find many publications and web-pages displaying empirical results, although there is a solid theoretical base backing up results and discussion on the conducted experiments. Most of which will mainly focus on distance (coverage) and signal power from the transmitter to the receiver. Unfortunately, there are important variables that are not taken into account in the majority of these experiments such as the channel where the signals are being propagated, other wireless transmissions that can interfere in the results, environment weather, and others.

About Wi-SUN, it is even harder to find papers and studies that relate directly to the results pursued in this dissertation. There is little focus on its performance against interference in recent studies and papers. Most researches focus on developing new methods to make the modulations within Wi-SUN (or 802.15.4g) better, algorithms to predict and counter interference, better synchronization, and such.

Finally, there are even fewer papers fairly comparing both technologies or approaching the questions about them with a systematic methodology. Most comparisons between these technologies are restricted to their specifications and data-sheets and are created by parts that want to promote one technology over the other.

To better understand how the theme is usually approached, a few of the studies, papers, and articles regarding LoRa's and Wi-SUN's performance and/or characteristics are summarized (while focusing on the subjects addressed by this dissertation) next, as they were of great importance and help to the writing of this dissertation.

In the article, A Study of LoRa: Long Range Low Power Networks for the Internet of Things [2], the authors introduce LoRa technology through an overview of

its main characteristics. The study brings a short, but in-depth analysis of LoRa components, explaining its physical layer and discussing them along with the text. After this discussion, the authors bring an experiment to the table in order to verify if the specified (and explained) performance of the LoRa receiver is actually reached in practice. Using a LoRa end-device and an industrial router as a gateway, they proceed to test the receiver sensitivity, shortly describing test conditions as: "the gateway was placed indoors, and the [end-]device was outdoors, in an urban environment" and giving details on the configuration of the used LoRa module. The results obtained were slightly above the specified values, as stated by the authors, and briefly discussed the experiment conditions. In the following section, a network coverage experiment is conducted. For this experiment, more details about the place and conditions (such as environmental temperature and ambient humidity) are stated, and also the positioning of the gateway and the end-device. Varying the location of the end-device and the spreading factor, the author correlates the package delivery ratio and chosen spreading factor with the distance between the end-device and the gateway, but there is no detail about the channel where the signals are propagated other than the previously described "urban environment". After a short discussion and explanation of how the LoRaWAN protocol would behave in such conditions, the study proceeds to give the readers an overview of the LoRaWAN protocol and its components. In the following sections, the LoRaWAN protocol is tested through new experiments to validate the protocol's behavior. In the conclusion, it is stated that LoRa modulation offers good resistance to interference, thanks to the chirp spread spectrum and high receiver sensitivity (which are bound to each other, since the sensitivity is a result of the processing gain given by the signal spreading). It is also stated that the modulation offers satisfactory network coverage up to 3 kilometers in a suburban area and that the spreading factor has a significant impact on the coverage. LoRa is then considered suited to low-power, low-throughput, and long-range networks.

In the paper IEEE 802.15.4g Based Wi-SUN Communication Systems [16], the authors introduce Wi-SUN communication systems through an overview of its main characteristics and in-depth explanation about their physical layers (PHY) and media access control (MAC) specifications, while also bringing computer simulation results to evaluate them both. Experimental results of the actual performance of IEEE 802.15.4g Wi-SUN devices under AWGN and multipath fading are also presented. The text begins with a light overview of how the physical layer specification of Wi-SUN is based on the IEEE 802.15.4g standard that defines alternate PHYs for, mainly, outdoor Low Data Rate Wireless Smart Metering Utility Networks. Following, the author explains how the Wi-SUN also includes media access control specifications and other characteristics such as adaptation, network, and transport layers standardized to support many applications

such as agriculture, intelligent transport systems, and disaster prevention. In the following section, it is explained, in a very thorough manner, the Wi-SUN communication systems, with a complete table of categories of these systems. Next, the IEEE 802.15.4g is brought to light with the modulations that are can be used within the standard. The following sections bring the characteristics of the IEEE 802.15.4g and IEEE 802.15.4e standards on a very detailed overview, and the Wi-SUN profiles are explained concluding the densest part of the paper. Following, the transmission performance experiment is detailed as the authors aim to measure PER curves for an IEEE 802.15.4g Wi-SUN device under AWGN and multipath fading environments. The setup for the experiment and the channel models that were used are presented, as well as the conditions for the experiment. The results are shortly discussed and shown as PER vs RSSI (received signal strength indication) curves. It is then stated, based on the results, that Wi-SUN modules achieve 10% PER, which is required by the standard, under one path channels and multipath fading environments with Doppler frequency of 0.4Hz at 920MHz. And then brings ideas for future studies involving multi-hop environments.

In Performance evaluation of LoraWan physical layer integration on IoT devices [17] the authors briefly introduce the Internet of Things (IoT) and mention a few emerging power-efficient IoT technologies such as ZigBee as they state that, although the high-power consumption options that we have deployed nowadays (GMS, LTE, WLANs and other) can be used for IoT connectivity, Low Power Wide Area Networks (LPWANs) is a promising alternative, as LPWANs have high coverage capabilities while maintaining low-power consumption. LoraWAN is then introduced by the study, and then it is explained that LoRa and LoRaWAN are not the same, as LoRa refers to the physical layer, while LoRaWAN is a communication protocol. A few more details about LoRa and the LoRaWAN power efficiency are given in the next section. The author then states that the LoRa modulation can be understood as a MFSK (Multiple Frequency-shift Keying) modulation on top of a Chirp Spread Spectrum (CSS), and explain that if the spreading factor is increased, the package size will be reduced, resulting in a higher power over the channel and longer communication distance. Following, a performance evaluation on LoRa's physical layer is performed. The text describes the PHY and details LoRa's parameters and how they affect the transmitted signal. Without a detailed explanation, the paper offers a figure composed by Bit Error Rate (BER) vs Signal to Noise Ratio (SNR) curves, for LoRa's different spreading factors (using a 125kHz bandwidth for every signal), as the result for a simulated experiment. While the results are discussed, the authors conclude that LoRaWAN is an ideal candidate for IoT applications and detail a few of LoRaWAN characteristics such as the high coverage capacity, adaptability, and low power consumption.

Addressing a subject related to Wi-SUN, the paper Experimental Interference Robustness Evaluation of IEEE 802.15.4-2015 OQPSK-DSSS and SUN-OFDM Physical Layers [18] experimentally evaluates the performance of the stated modulations against different types of interference, aiming to provide a comprehensive analysis and results in terms of packet delivery ratio. The paper starts by introducing the IEEE 802.15.4 and the IEEE 802.15.4g standards while bringing more details about the SUN-OFDM and its benefits. In the following sections, OQPSK-DSSS is briefly explained, and the SUN-OFDM has its characteristics and parameters explained and discussed in-depth. The methodology and setup used to evaluate the modulations are then presented by the authors in a very detailed manner. For the measurement procedure, the authors chose to use each one of the selected modulations (OFDM1-MCS1, OFDM2-MCS2, OFDM3-MCS3, OFDM4-MCS5, OQPSKDSSS) as an interference signal against all others, and they also repeated the experiment for two different lengths of payload. Following, the Package Delivery Ratio (PDR) is defined in the text as the percentage of packets successfully received under the presence of interference. The text proceeds to detail the relevant components and concepts around the experiment and giving more details about the setup and equipment used to achieve the desired results. In the section dedicated to the results, a few figures displaying the obtained curves of PDR are shown and briefly discussed. Authors proceed to widely discuss the obtained results and compare them to the data-sheets and also to each other (the curves for different modulations). The conclusion of this study states that the SUN-OFDM physical layer provides significant benefits compared to OQPSK-DSSS, as the SUN-OFDM modulation presented higher levels of robustness in all the experiments while occupying a narrower bandwidth, which results in higher spectral efficiency. Overall, it is stated that the SUN-OFDM physical layer is suitable for deployment in low-power wireless networks in industrial scenarios and should be considered for such applications.

Performance of a low-power wide-area network based on LoRa technology: Doppler robustness, scalability, and coverage [19] is an article that reports experimental results and validations of LoRa technology while discussing the obtained data. The text begins by introducing Low Power Wide Area Networks, as it is stated that LPWANs represent a new trend in telecommunication and it is designed to enable a broad range of Internet of Things applications. The authors briefly compare LPWANs to existing communication technologies and give an overview of LPWANs. Following, the article provides an overview of the LoRaWAN protocol, detailing its physical layer, link layer, and network architecture. In the following section, a discussion of the LoRaWAN performance against the Doppler effect is made, along with an analysis of LoRaWAN's throughput and network capacity. After a brief explanation backed by a few interesting equations, the authors explain that the frequency shift caused by the Doppler effect causes the auto-

correlation peak to shift in time, which can utterly affect packet reception, but if the chirp rate is large enough this time shift will be too small to be taken in account. The article proceeds to discuss the end-devices maximum throughput and LoRaWAN's scalability and network capacity. In the following section, three experiments to evaluate the practical capabilities of LoRa are presented. The first two experiments were conducted to investigate the performance of LoRa end-devices under the Doppler shift, focusing on the highest spreading factor offered by the technology. The setup and methods are explained in detail and the results are presented along with the discussion, where it is stated that when relative speed between devices exceeds 40 kilometers/h, LoRa's communication performance deteriorates. In the following experiment, the coverage of LoRaWAN is investigated, by mounting an end-device on the roof-rack of a car and the mast of a boat while driving and sailing around the gateway which had a fixed position at the University of Oulu, in Finland. The results of this last experiment showed that using the highest spreading factor LoRa can offer, 62% of the packets were successfully delivered within a 30 kilometers range. Authors then state that LoRa has the potential to become a wireless communication enabler for a variety of IoT applications as it can be used for low-cost power-efficient long-range wireless communications.

In the paper Path Loss Models for Low-Power Wide-Area Networks: Experimental Results using LoRa [20], authors chose to evaluate the accuracy of Received Signal Strength Indication (RSSI) of LoRa chipsets in a laboratory. The text introduces LPWAN and shortly describe its scenario on Europe, while also introducing LoRaWAN and a few example applications in which the technology can be used. Following, the Path Loss Models are described and shown as the contribution of related works mentioned in the text. As the paper goes on, the experimental setup is detailed as a Fixed LoRa transceiver on the roof of the university and a moving transceiver installed on a car at 1.2-meter height, results are not discussed at this time. The authors then decided to test the reliability of the reported values of RSSI by building up a small laboratory experiment in which a spectrum analyzer was used to measure the channel power while the signal was attenuated (with dynamic attenuators) in a setting supposed to simulate the path-loss. After a brief discussion on the obtained results, and the authors explain the data acquisition process and create a table of GPS locations and signal strength as a result of their experiment. Following, the results are discussed and experimental data is compared to data generated by the previously described models. Authors conclude that no model was perfect when compared to the practical results and assume the accuracy can be increased by calculating reflections and diffraction from buildings and terrain irregularities.

The paper Experimental Performance Evaluation of LoRaWAN: A Case Study in Bangkok [21], presents an experimental performance evaluation of LoRaWAN in a real-

world environment. First, introducing the concept of the Internet of Things, the authors explain how Wi-Fi and Cellular Communications were the preferred communication technologies to use in Internet of Things applications, but as new technologies arise with long-range coverage capabilities and low-power consumption, such as LoRaWAN and Narrow Band IoT (NB-IoT), they take the spotlights. The study describes LoRa as a physical layer that uses Chirp Spread Spectrum modulation techniques and states that LoRa is used in LoRaWAN network protocol, which has features such as 15 kilometers coverage capacity in the countryside, low-power consumption allowing for 10 years of battery life (without detailing the applications in which this is possible) and low data rates. The paper mentions that LoRaWAN architecture is typically organized in 'star-of-stars' topology and proceeds to explain the topology. Following, the text brings up the device classes of LoRaWAN, summarizing each of the classes by their main characteristics. In the performance evaluation section, the tested devices (gateway and end-device) are detailed and the experimental results are illustrated as Packet Loss vs Distance curves. The experiment conditions are briefly mentioned as the authors explain the positioning of the devices. The authors conclude that, although LoRaWAN specifications state that it can reach between 2 kilometers and 5 kilometers of coverage range in urban environments and 15 kilometers in rural environments, the results show that the range is only up to 55 meters to 110 meters in an indoor urban environment, and only up to 2 kilometers in outdoor rural areas. The paper also states that the communication range is influenced by the properties of the antennas such as gain, direction (although they also state that an omnidirectional antenna was used in the experiments), and height above the surrounding landscape. The end of the final section brings future work proposals in which antenna parameters, environmental characteristics (such as humidity and temperature) will also be analyzed alongside with power consumption measurements.

Many works, papers, and studies bring very interesting experimental results about both technologies, but without mentioning all the conditions that surround their experiments, making it difficult to understand why a few of those results were so controversial, even after discussing possible reasons for the measurements and outcomes of the tests. The theoretical discussions in these texts are very helpful and they tend to complement each other as there are several details that can go unnoticed while studying such a complex theme.

This dissertation is not focused on the theoretical analysis of the technologies, although it shortly presents both LoRa and Wi-SUN and their characteristics. The contributions added by this work are the methodologies that can be used to evaluate the modulation's performance systematically, always repeating the same experimental conditions, and the measurements and test results for two of the most promising emerging

technologies for the Internet of Things, specifically Low Power Wide Area Networks, in the market, so that they can be compared in a fair way, without depending on location, weather, moving speed or other variables that can affect further analyses. Although many of the papers presented in this section bring important results and valuable data to the discussion, a few questions remain unanswered when comparing the technologies side-by-side, which is what is addressed in the next chapters of this text.

1.1 Motivation

Although theoretical and practical results of the tested integrated circuits can be easily found, they still lack the systematic approach component that would allow a fair comparison between them and the technologies they carry. In order to make it easier to choose between circuits, technologies, and modulation schemes, the introduction of a standardized testing method, and the testing method itself, is presented alongside with the results collected for two of the most promising technologies for Low Power Wide Area Networks, allowing for them to be compared side-by-side.

1.2 Objectives

This dissertation's main objective is to compare, in a fair fashion, two of the most promising LPWAN technologies available in the market at the moment, based on real testing results. Another goal is to collect data of the tested integrated circuits, as well as of the technologies and modulations they provide, on how they behave in real-world-like environments, enabling future analysis.

1.3 Contributions

A few humble contributions are provided by this dissertation, such as the testing methods and how to conduct the experiments, the data, and results collected during the experiments, and a comparison between the tested technologies. The studies and results may also be used to conceive papers on the subjects of Low Power Wide Area Networks, LoRa, the IEEE 802.15.4g standard, Wi-SUN, Internet of Things, and others that are, currently, in the spotlight of researchers, manufacturers, and enthusiasts around the globe.

1.4 Dissertation Outline

This dissertation is formatted as a technical report on the experimental procedures that were used to obtain the results discussed at the end of each related chapter, and it is divided into four chapters. Chapter 2 intends to introduce the technologies that will be explored through this work, hoping to level the knowledge of the reader about the main characteristics of these technologies and how they work. Chapters 3 and 4 report experiments done by exploring the setups built, the methods used, and presenting a light discussion about the results that were obtained. Chapter 5 brings the conclusions and considerations about the results discussed in the previous chapters, bringing future work proposals to complete the tests.

2 IoT, LoRa and Wi-SUN

2.1 Introduction

This chapter should provide basic and relevant information about the Internet of Things (IoT), LoRa, and Wi-SUN to make it easier to understand the motivations of this work and to provide other details that will help the comparison between the target-technologies.

2.2 Internet of Things

Internet of Things, or simply IoT, is the concept of connecting any device to other devices through the internet. If a lamp is connected to a cellphone or a washing machine and they can send messages or data to one another, it is IoT. In a very simple way, IoT allows us to connect any device with a power switch to other devices, creating a, potentially infinite, network of all sorts of gadgets and even people. By 2020 it is estimated that over 26 billion devices will be connected [22], forming this massive IoT network.

Connecting so many devices would make life easier in many ways. We can already know, beforehand, if something is going to spoil in our fridge, or even if we are running out of milk - and it is the fridge that told us about this. Now, if the fridge is connected to the internet, it could order another gallon of milk, and we would not have to worry about running out of milk, or anything, at home. This concept can be expanded to almost every aspect of every-day life. To programmers, for instance, it means that they will always have warm coffee to drink because their computers will notify the coffee maker whenever they start coding something. Endless opportunities come from IoT and they should be explored to its fullest.

Thinking on much larger scales, IoT enables Smart Cities, which can help humanity to improve the usage of resources such as electrical energy and fuel while reducing waste of all kinds. It can also help with sustainability issues by improving transportation logistics and reducing our carbon footprints.

IoT is a growing topic all over the world and it is already impacting our lives in so many ways. It brings many opportunities as the network grows bigger and more connected. The next steps should be towards a better, more reliable, and efficient society where sensors and other devices can give us even more data and insights about the world and how we can use technology to make it a better place.

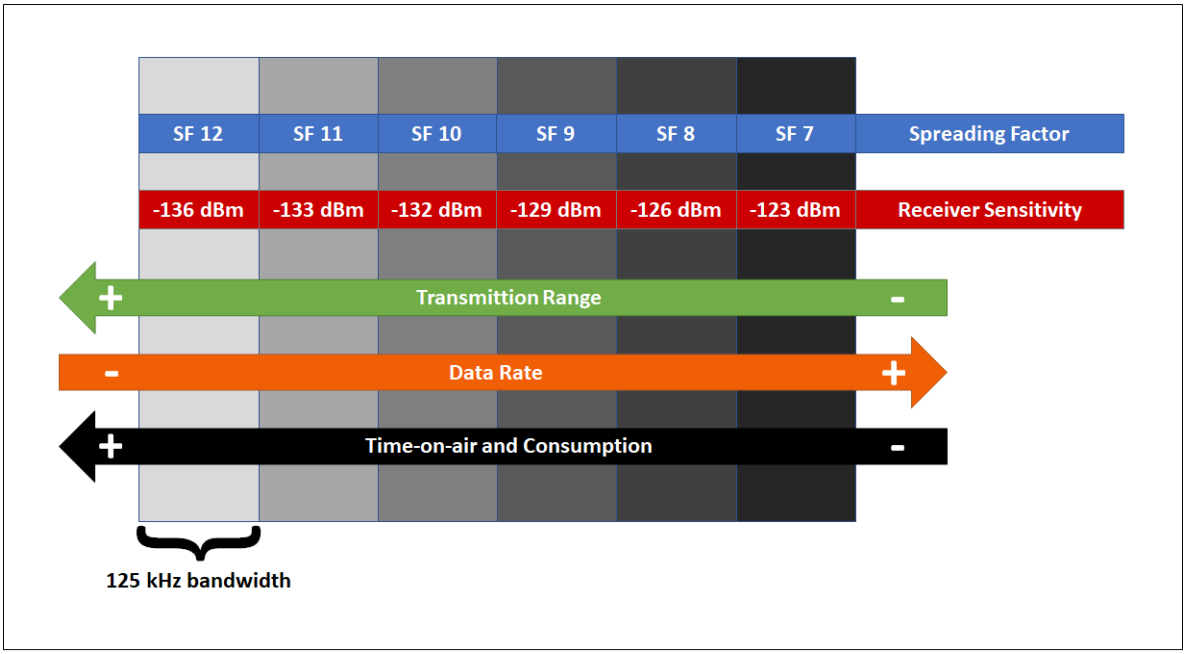

Figure 2.1 – Impact of LoRa Parameters on Transmission Distance and Throughput. Based on LoRaWAN 101 - A Technical Introduction [1]

2.3 LoRa

2.3.1 LoRa Introduction

LoRa, which means "Long Range", is a proprietary technology for communication and networks. Developed by Semtech, LoRa main focus is LPWANs (Low Power Wide Area Networks) [2]. LoRa implements the physical layer to create links for long-range communications. This technology uses Spread Spectrum Modulation, or Chirp Spread Spectrum to be exact, which can increase sensitivity, given a fixed bandwidth while decreasing data rates [23]. Its main objective is to achieve long-range communication with very low power consumption.

Almost all LoRa parameters are customizable, but some are more relevant because they directly influence communication distance and data transfer rate, such as bandwidth, spreading factor, and forward error correction code, this last parameter defines data redundancy and correction of a limited number of errors in the messages received by a LoRa device [2]. Fig. 2.1 shows how spreading factor and bandwidth influence data transfer rate, transmission distance, and the time it takes for the message to be transmitted.

2.3.2 Spread Spectrum and LoRa Spread Spectrum

To start talking about spread spectrum techniques, first, we must briefly recapitulate the Shannon-Hartley theorem. The theorem defines the maximum data rate within a fixed bandwidth in the presence of noise interference and establishes Shannon's

channel capacity for a single communication link [23]. Shannon's channel capacity is depicted in Eq.(2.1), where C is the maximum achievable data rate (in bits/sec), B is the bandwidth of the signal (in Hz), S is the signal power (in Watts) and N is the Noise Power (in Watts).

$$\mathrm{C} = \mathrm{B} \log \left(1 + \frac{S}{N}\right) \tag{2.1}$$

For spreading spectrum applications the ratio between signal and noise $\frac{S}{N}$ is very small, therefore $\log(1 + x) \approx x$, and therefore it is possible to write (2.1) as

$$\frac{N}{S} = \frac{B}{C} \tag{2.2}$$

From (2.2), considering that C is fixed, if the signal to noise ratio decreases, implies necessarily that we must have an increase in the bandwidth B.

What spread spectrum techniques try to accomplish, is to increase the bandwidth of a signal by deliberately spreading it in the frequency domain, thus resulting in a signal with a considerably larger bandwidth. This makes the transmitted signal more resistant to interference and noise.

In Direct Sequence Spread Spectrum (DSSS) systems, the amount of spreading depends on a ratio of "chips per bit". A chip is a pulse of a DSSS code (like a binary code) which is multiplied by a data sequence to achieve the wanted spreading. The relation between the chip sequence and the wanted data rate of a signal is called processing gain (G_p) shown in (2.3) given in dB as

$$G_p = 10 \log_{10} \left(\frac{R_c}{R_b}\right). \tag{2.3}$$

Note that, in (2.3), R_c is the chip rate (in chips per second) and, R_b, the bit rate (in bits per second). The processing gain enables the receiver to recover parts of the data sequence correctly, even for signal-to-noise ratios with negative values. In LoRa modulation, the technique used is the Chirp Spread Spectrum, which generates a chirp signal, with varying frequency. The data signal is chirped, similar to the DSSS technique, but is then modulated into a chirp signal [23]. The associated bit rate, R_b, for such modulation can be defined as in (2.4), where SF is the Spreading Factor (varying from 7 to 12) and BW is the Modulation Bandwidth.

$$R_b = SF \frac{1}{\frac{2^{SF}}{BW}} \tag{2.4}$$

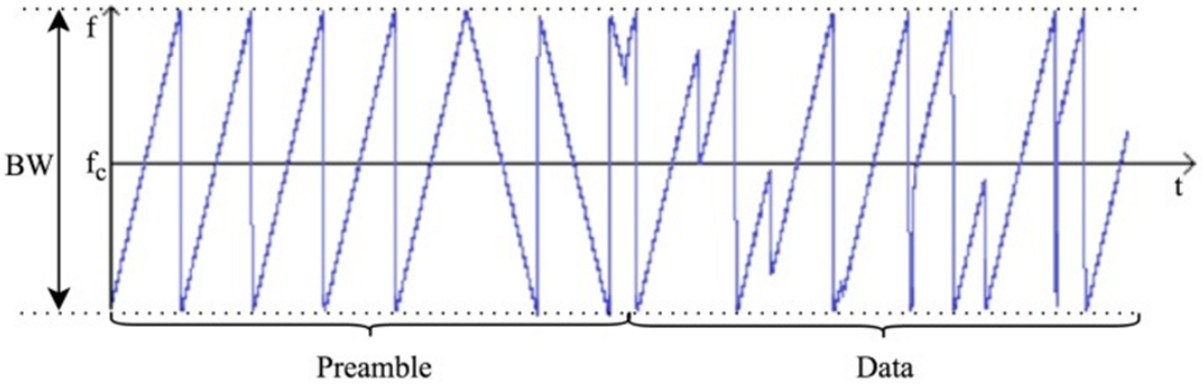

Figure 2.2 – Frequency variation over time of a signal emitted by a LoRa transmitter, where f_c is the center frequency of the channel, and BW is the bandwidth [2].

LoRa modulation includes a variable error correction scheme for improving the robustness of a given signal. Thus, the nominal bit rate should be defined as in (2.5), where CR is the Code Rate (varying from 1 to 4).

$$R_b = SF \frac{\frac{4}{4+CR}}{\frac{2^{SF}}{BW}} \tag{2.5}$$

It is possible to notice that LoRa is able to achieve a higher level of robustness at the expense of lower data rates and a wider bandwidth, which is related to the spread spectrum [23].

2.3.3 LoRa Physical Frame

LoRa modulation is a proprietary technology and is not completely open information-wise. Therefore it is important to note that the facts presented below are based only on published information about the technology. Although LoRa can transmit arbitrary frames, physical frames have a specified format that is implemented in Semtech transceivers. During frame transmission, it is important to note that the spreading factor and bandwidth remain constant. LoRa frames start with a preamble, which is formed by a constant upchirps sequence that covers the entire frequency band[2]. The last two upchirps encode a sync word. The sync word is a byte used to differentiate LoRa networks that use the same frequency band. This means that if a device decodes a sync word other than the expected setting, it immediately stops listening to the received data. The sync word is followed by 2.25 downchirps, during 2.25 symbols. This preamble can be set to last from 10.25 symbols to 65539.25 symbols [2]. A graphical representation of the chirps can be observed in Fig. 2.2.

After the preamble, you can send an optional header. When present, the header

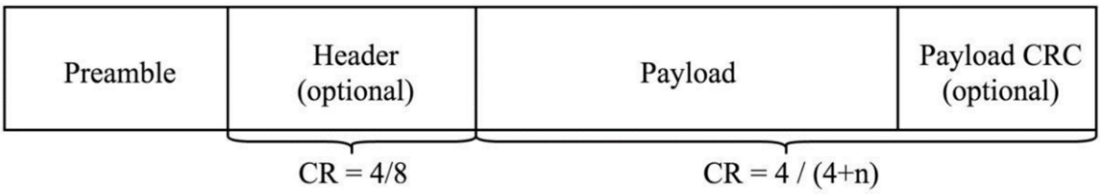

Figure 2.3 – Graphical representation of a LoRa Frame [2].

is always transmitted with a code rate of $4/(4+n)$ for n equals to 1, 2, 3, or 4, which determines data redundancy and minimizes errors in the final reading. This header indicates the payload size (in bytes), the code rate used during the rest of the transmission, and whether or not there is a 16-bit cyclic redundancy check (CRC) for the payload at the end of the frame [2]. The header also includes a CRC to allow the receiver to discard packets with invalid headers. The payload size is stored using only one byte. The payload is sent right after the header, and at the end of the frame is located the optional CRC. Fig. 2.3 shows an example of LoRa frame.

2.3.4 LoRaWAN and LoRa Alliance

LoRa Alliance is a non-profit organization whose members are involved in the design and use of the LoRaWAN protocol [24]. LoRaWAN is a protocol created for LPWAN, using LoRa in the physical layer. This protocol aims at maximum optimization in terms of energy consumption and effective communication [1]. To make this possible, it makes adjustments to the spreading factor, channel switching, and even automatically adjusts the bandwidth and calibrates the signal strength. LoRaWAN also determines classes for devices connected to the network, and these devices are classified as A, B, or C (the characteristics of each class are summarized in table 2.1), depending on the type of activity they are part of [1]. Classes function as a priority system, where a given class has more bandwidth, time on-air, and adjustments to other parameters that determine the size and amount of messages that can be sent by devices. This helps optimize network performance and lower power consumption for devices that do not necessarily need to send hundreds of messages a day. LoRaWAN also implements network security. This security is based on the IEEE 802.15.4 (Low Rate WPAN) standard, with the addition of Network Session Key and Application Session Key [1]. Since low power devices do not have good bidirectional communication capabilities, more complex security protocols become impracticable, even implementing encryption keys is difficult. Therefore, LoRaWAN's security is relatively weak and may not be sufficient for certain activities, although it is acceptable for conventional Internet of Things (IoT) activities. In short, LoRaWAN has a simple star topology, low transfer rate, long battery life for devices, and long communication distance. LoRaWAN is a protocol to consider for IoT, machine-to-

Device Class	Summary
Class A	* Bidirectional communications * Unicast messages * Small payloads * Long intervals * End-device initiates communication (uplink) * Server communicates with end-device (downlink) during predetermined response windows
Class B	* Bidirectional with scheduled receive slots * Unicast and Multicastmessages * Small payloads * Long intervals * Periodic beacon from gateway * Extra receive window (ping slot) * Server can initiate transmission at fixed intervals
Class C	* Bidirectional communications * Unicast and Multicastmessages * Small payloads * Server can initiate transmission at any time * End-device is constantly receiving

Table 2.1 – Summary of LoRaWAN device classes characteristics [1]
.

machine, industrial automation, low power application, battery-powered sensors, smart cities, agriculture, and other low rate communication activities.

2.3.5 LoRa's Market

With a global ecosystem and over 10,000 networks around the world, LoRa has captured a significant chunk of the IoT market. The advantages of this technology have attracted thousands of developers and the world's largest network operators. The LoRa Alliance currently has over 500 members with the goal of facilitating the mass adoption of LoRa. LoRaWAN-based networks are spreading around the world fast. Several countries in Europe are already completely covered by the technology and many others are on their way to achieve the same. Japan and the United States are also on the list of countries that will be covered by the technology.

In South America, Argentina has already completed the deployment of network infrastructure and is soon expected to have thousands of devices connected using LoRa

[25].

In Brazil, the virtual mobile operator specialized in IoT, NLT (Next Level Telecom), signed a contract to use American Tower (ATC) LoRa network. The expectation is that LoRa will help monitoring fleets and cargo, as well as power smart cities and agribusiness in the country [26]. The metro area of at least three Brazilian capitals (São Paulo, Rio de Janeiro, and Belo Horizonte) is covered by ATC's LoRaWAN-based network. Semtech's Director of IoT, Vivek Mohan, believes that ATC's deployment in Brazil will enable smarter IoT solutions in the country [27]. The IoT market for applications and hardware is expected to generate US$3.2bn in Brazil by 2021 [25].

While the focus is on public networks, private networks are also an essential component of the LoRa ecosystem. Some predictions indicate that by 2022, LoRa private networks will be approximately two-thirds of the ecosystem [28]. LoRa is a great promise that should develop in the coming years, leveraging the IoT market a little further.

2.4 Wi-SUN and IEEE 802.15.4g Standard

2.4.1 Wi-SUN Introduction

Wireless Smart Utility Network, or Wi-SUN, is a communication technology designed for IoT, Smart Utilities (as the name suggests), and Smart Cities. Smart metering is one of the areas that have been benefiting the most from Wi-SUN because the technology can automatically and effectively transmit the measured data to a database through multi-hop relaying operations. This way, all the collected data can be analyzed and then used to control resource consumption, for example, in a building.

While all technical specifications are determined by the Wi-SUN Alliance, the specification of Wi-SUN PHY (physical layer) is, mainly, based on IEEE 802.15.4g, which defines a PHY specification for outdoor low data-rate wireless smart metering networks [16]. Wi-SUN also supports several applications through specifications of media access control (MAC), adaptation protocols for transport layers that are standardized by IEEE.

2.4.2 IEEE 802.15.4 and the IEEE 802.15.4g Amendment

With its initial version in 2003, the IEEE 802.15.4 standard has been updated through a number of releases and variants to meet different applications, forms of the physical layer, data rates, and other characteristics. Table 2.2 summarizes IEEE 802.15.4 releases and amendments.

IEEE 802.15.4g defines an amendment to IEEE 802.15.4 that addresses, among

IEEE 802.15.4 VERSION	DETAILS AND COMMENTS
IEEE 802.15.4 - 2003	This was the initial release of the IEEE 802.15.4 standard. It provided for two different PHYs - one for the lower frequency bands of 868 and 915 MHz, and the other for 2.4 GHz.
IEEE 802.15.4 - 2006	This 2006 release of the IEEE 802.15.4 standard provided for an increase in the data rate achievable on the lower frequency bands. This release of the standard updated the PHY for 868 and 915 MHz. It also defined four new modulation schemes that could be used - three for the lower frequency bands, and one for 2.4 GHz.
IEEE 802.15.4a	This version of the IEEE 802.15.4 standard defined two new PHYs. One used UWB technology and the other provided for using chirp spread spectrum at 2.4 GHz.
IEEE 802.15.4c	Updates for 2.4 GHz, 868 MHz and 915 MHz, UWB and the China 779-787 MHz band.
IEEE 802.15.4d	2.4 GHz, 868 MHz, 915 MHz and Japanese 950 - 956 MHz band.
IEEE 802.15.4e	This release defines MAC enhancements to IEEE 802.15.4 in support of the ISA SP100.11a application.
IEEE 802.15.4f	This will define new PHYs for UWB, 2.4 GHz band and also 433 MHz
IEEE 802.15.4g	This will define new PHYs for smart neighbourhood networks. These may include applications such as smart grid applications for the energy industry. It may include the 902 - 928 MHz band.

Table 2.2 – IEEE 802.15.4 Standard Summary [5].

other things, outdoor low data-rate wireless smart metering utility network requirements. There are three PHYs adopted by the 802.15.4g standard, which are the multi-rate and multi-regional FSK (MR-FSK), MR-O-QPSK, and MR-OFDM.

2.4.3 IEEE 812.15.4g Physical Frame

The IEEE 802.15.4g defines alternate physical layers (PHYs) and MAC modifications that are required to support the PHYs implementation. Fig 2.4 and Fig 2.5 show the configuration of the physical layer convergence protocol data unit (PPDU) formats determined by IEEE 802.15.4g.

2.4.4 Wi-SUN Alliance

The Wi-SUN Alliance is a global ecosystem of Corporations and World Leaders in Smart Utility, Smart City and Internet of Things Markets [29] from Australia, Brazil, Canada, China, Europe, India, Japan, Korea, Singapore, and the United States.

Focusing mainly on applications such as Distribution Automation, Advanced Metering Infrastructure, and even Home Energy Management [30], the alliance provides mesh solutions for Field Area Networks (FANs) using Wi-SUN as the wireless solution.

		Octets	
		2	Variable
Preamble	SFD	As defined in 18.1.1.3	PSDU
SHR		PHR	PHY payload

Format of the MR-FSK PPDU (without mode switch)

		Octets
		2
Preamble	SFD	As defined in 18.1.1.4
SHR		PHR

Format of the MR-FSK mode switch PPDU

18.1.1.3 PHR (without mode switch)

Bit string index	0	1–2	3	4	5–15
Bit mapping	MS	R_1–R_0	FCS	DW	L_{10}–L_0
Field name	Mode Switch	Reserved	FCS Type	Data Whitening	Frame Length

Figure 114—Format of the PHR (without mode switching) for MR-FSK

Table 133—Relationship between FCS Type field and transmitted FCS length

FCS Type field value	Transmitted FCS length
0	4-octets
1	2-octets

18.1.1.4 PHR for the mode switch packet

Bit string index	0	1–2	3	4–10	11–14	15
Bit mapping	MS	M_1–M_0	FEC	As defined in Figure 116	B_3–B_0	PC
Field name	Mode Switch	Mode Switch Parameter Entry	New Mode FEC	New Mode	Checksum	Parity Check

Figure 115—Format of the PHR for MR-FSK mode switching

Figure 2.4 – PPDU format of IEEE 802.15.4g MR-FSK [3].

		Number of OFDM Symbols			
		Variable	Variable	6 bits	Variable
STF	LTF	As defined in 18.2.1.3	PSDU	TAIL	PAD
SHR		PHR	PHY payload		

Format of the MR-OFDM PPDU

		Octets	
		3	Variable
Preamble	SFD	As defined in 18.3.1.3	PSDU
SHR		PHR	PHY payload

Format of the MR-O-QPSK PHY PPDU

18.2.1.3 PHR

The PHR consists of the Frame Length field and frame control bits. The PHR structure shall be formatted as illustrated in Figure 131. All multi-bit fields are unsigned integers and shall be processed MSB first.

Bit string index	0–4	5	6–16	17–18	19–20	21	22–29	30–35
Bit mapping	RA_4–RA_0	R	L_{10}–L_0	R_1–R_0	S_1–S_0	R	H_7–H_0	T_5–T_0
Field name	Rate	Reserved	Frame Length	Reserved	Scrambler	Reserved	HCS	Tail

PHY header fields for MR-OFDM

18.3.1.3 PHR

The format of the PHR is shown in Figure 141. All multi-bit fields are unsigned integers and shall be processed MSB first.

Bit string index	0	1	2	3	4	5–15	16–23
Bit mapping	SM	RM_1	RM_0	R_1	R_0	L_{10}–L_0	H_7–H_0
Field name	Spreading Mode	Rate Mode		Reserved		Frame Length	HCS

Figure 141—Format of the PHR for MR-O-QPSK

Figure 2.5 – PPDU formats of IEEE 802.15.4g MR-OFDM and MR-O-QPSK [3].

Their FANs deliver multi-vendor interoperable solutions for a broad range of applications that can enable Smart Cities, such as traffic management and street lighting.

The Wi-SUN alliance seeks to advance Wi-SUNs all around the globe alongside with interoperability and compliance certification programs while promoting the adoption of open industry standards for Wireless Smart Utility Networks and all related applications.

2.4.5 Wi-SUN's Market

Wi-SUN has been growing in the smart cities and smart utilities markets, because it is an alternative for low-power wide-area networks (LPWAN).

Wi-SUN alliance announced its first wave of products with Wi-SUN FAN in 2019. This means that approved products can now display the Wi-SUN certified FAN logo and let customers know that these devices are compliant with the standards defined by the alliance.

Although Wi-SUN had been quietly gaining market over the years, the last months seem to have come to change this scenario. The open mesh protocol proposed focus on untangling the net of communication technologies that have grown invariably around proprietary and systems and legacy equipment [31].

With the adoption rates of IoT growing every day, Wi-SUN Alliance members are experiencing a higher demand for their products, especially in the fields that are rolling out applications such as smart metering, general smart utilities, and smart cities.

3 Sensitivity and Additive White Gaussian Noise Performance

3.1 Introduction

In this chapter, experimental procedures for obtaining sensitivity and the performance of networking devices in additive Gaussian white noise are presented along with methods and equipment setups, which are proposed to create a controlled testing environment, in order to achieve fair conditions for systematically compare these devices and the technologies they use.

3.1.1 Characteristics and Parameters

Table 3.1 shows the most commonly applicable MR-FSK parameters, table 3.2 presents the main parameters of LoRa, and tables 3.3 to 3.5 bring the main parameters of IEEE 802.15.4g. Those parameters will be explored in the following sections, during the evaluation of the integrated circuit.

Parameter	**Operating Mode 1**	**Operating Mode 2**	**Operating Mode 3**
Data Rate (Kbps)	50	150	200
Modulation	Filtered 2FSK	Filtered 2FSK	Filtered 2FSK
Modulation Index	1	0.5	0.5

Table 3.1 – MR-FSK Parameters for Most Commonly Applicable Regulatory Domains.

Mode LoRa CSS	**Bandwidth [kHz]**	**Spreading Factor**	**Coding Rate**	**Data Rate [Kbps]**
SF7-BW500	500	7	4/5	21.875
SF10-BW500	500	10	4/5	3.906
SF12-BW500	500	12	4/5	1.172
SF7-BW250	250	7	4/5	10.938
SF7-BW125	125	7	4/5	5.469
SF12-BW125	125	12	4/5	0.293
SF7-BW250-CR8	250	7	1/2	6.836

Table 3.2 – LoRa Parameters.

Parameter		Option			
		1	**2**	**3**	**4**
Bandwidth [kHz]		1094	552	281	156
Data Rate	MCS0 [Kbps]	100	50	-	-
	MCS1 [Kbps]	200	100	50	-
	MCS2 [Kbps]	400	200	100	50
	MCS3 [Kbps]	800	400	200	100
	MCS4 [Kbps]	-	600	300	150
	MCS5 [Kbps]	-	800	400	200
	MCS6 [Kbps]	-	-	600	300

Table 3.3 – MR-OFDM Main Characteristics.

MCS	Modulation	Code Rate	Frequency Spreading
0	BPSK	1/2	4x
1	BPSK	1/2	2x
2	QPSK	1/2	2x
3	QPSK	1/2	No Spread
4	QPSK	3/4	No Spread
5	16-QAM	1/2	No Spread
6	16-QAM	3/4	No Spread

Table 3.4 – Modulation and Coding Schemes for MR-OFDM.

Mode O-QPSK	CR100-RM0	CR2000-RM0
Chip Rate [Kchip/sec]	100	2000
Bandwidth [kHz]	100	2000
Spreading Factor	8	32
Code Rate	1/2	1/2
Data Rate	6.25	31.25

Table 3.5 – MR-O-QPSK Parameters.

3.2 Experimental Procedures

3.2.1 Materials and Equipment

The main goal of this experiment was to systematically test the modulation technologies in a controlled environment. To create such conditions, the equipment and other necessary materials are listed below:

- 02 Atmel AT86RF215 – 802.15.4g Transceiver
- 02 Semtech SX1276 915MHz – LoRa Transceiver
- 01 Laptop with MATLAB
- 01 Spectrum Analyzer – Agilent E4404B

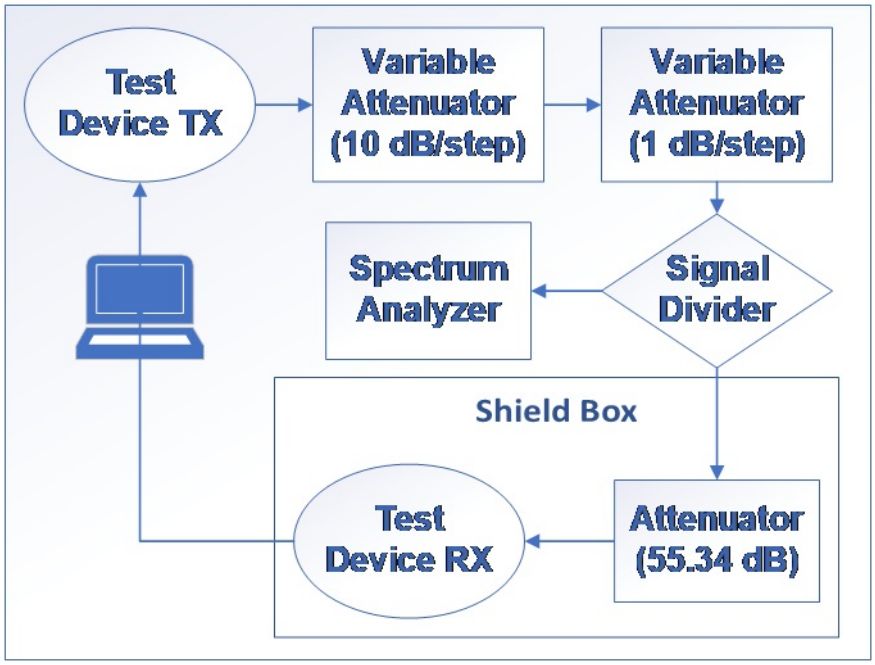

Figure 3.1 – Flow chart representing the setup necessary to measure the sensitivity of a device.

- 01 Signal Generator – Keysight N5172B
- 01 Shield Box
- 02 Variable Attenuators (10 dB/step and 1dB/step)
- 01 In-line Attenuator (55.34 dB)
- 02 Signal Divider and Combiner
- Miscellaneous Adapters
- Cables for the necessary connections

It is important to state that not all equipment nor materials were used for every single one of the experiments. The setup for each experiment is described in their respective section.

3.2.2 Sensitivity Experiment

The sensitivity is the measure of the capacity of a receiver to detect a signal that is weak in power. It is important to measure the sensitivity of the used receivers to determine the quality of the implementation of the transceivers and the boards that carry them. To measure the sensitivity, the equipment and materials were set as shown in Fig. 3.1.

Initially, both the receiver and transmitter boards were configured to use the same communication parameters. Next, the transmitter was commanded to send data packets in 'burst' mode to the receiver. To clarify the 'burst' mode: the signal was continuously transmitted for a certain amount of time and then was interrupted for a short period just to be transmitted again, and that cycle was repeated during the experiment. Using the laptop, it was observed how many of those packets arrived at the receiver and how many of those were actually correct. With this information, it is possible to determine the PER (Package Error Rate) between transmitter and receiver. The package error rate is defined by the percentage of packages that the receiver misread. If at least on bit of a package was read wrongly (1 when it should be 0 or 0 when it should be 1) that package was considered wrong and was added to the PER. Following, the variable attenuators were used to lower the signal power at the input of the receiver to the point where it was possible to measure a PER equal to or lower than 10%, meaning that the number of wrong packets should be as close to 10% as possible, but never surpass this upper boundary. The next step was to configure the spectrum analyzer. For the GFSK signals, the spectrum analyzer was adjusted to use the center frequency and the full bandwidth of the studied signal, using a resolution bandwidth of 1kHz. While for the other signals, considered flat within their 3dB bandwidth (e.g. CSS, OFDM, and O-QPSK), the spectrum analyzer was configured to use the center frequency of the observed signal, but only 20% of its total bandwidth and a resolution bandwidth of 1kHz. Using this method, it was possible to avoid measuring the valleys caused in the spectrum when the signal was interrupted due to the 'burst', accomplishing a fairer experiment. Next, the channel power was measured using the spectrum analyzer in the moments when the signal was present in the whole measured bandwidth. For each signal, 10 measurements were made and then averaged to obtain the channel power. Since the flat signals had only 20% of their bandwidth measured, it is necessary to calculate the channel power for the full bandwidth of these signals. To do so, 6.9897 dB were added to the measured power. This value corresponds to the expansion of the channel power of a 20% bandwidth to 100% of the bandwidth and is given by (3.1).

$$\text{Calculated Channel Power} = \text{Measured Channel Power} + 10\log_{10}\left(\frac{100}{20}\right) \quad [\text{dBm}] \tag{3.1}$$

As shown in Fig. 3.1, there was an in-line attenuator positioned between the receiver and the transmitted signal. This attenuator was previously characterized by the experiment and the total attenuation provided by it was 55.34 dB. To determine the sensitivity of the signals, it is necessary to subtract this attenuation from the already

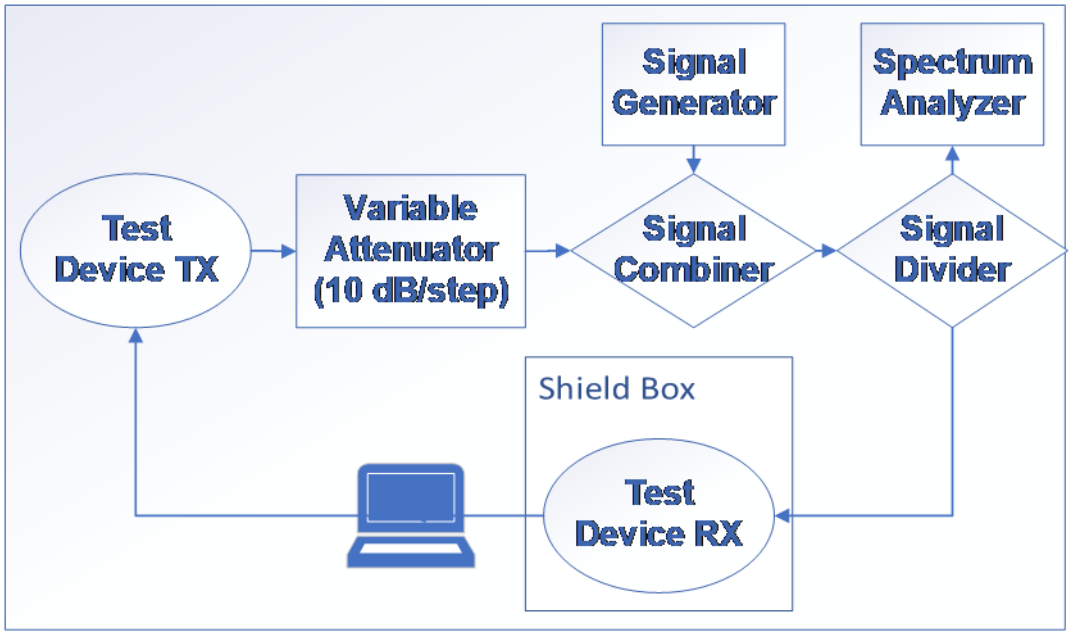

Figure 3.2 – Flow chart representing the setup to measure the PER performance of a device under Additive White Gaussian Noise.

measured and calculated values, as shown in (3.2).

$$\text{Sensitivity} = \text{Calculated Channel Power} - 55.34 \quad [\text{dBm}] \tag{3.2}$$

3.2.3 Additive White Gaussian Noise Experiment

The AWGN performance experiment determines how robust a modulation is to noise interference. This experiment consists of adding an AWGN signal to the transmitted signal and measuring how many packets arrived flawlessly at the receiver. To measure the AWGN performance, the equipment and materials were set as shown in Fig. 3.2.

First, both transmitter and receiver were configured to use the same communication parameters. Next, the transmitter was commanded to send an infinite sequence of messages composed of packets of 100 octets (800 bits), in 'burst' mode. The spectrum analyzer was configured to measure the channel power of the whole bandwidth of the targeted signal, using the same center frequency as of the signal and a resolution bandwidth of 1 kHz. After measuring the channel power of the signal, the transmission was interrupted.

Using the signal generator, an AWGN signal was added to the system. This signal had the same center frequency and the same bandwidth as the evaluated modulated signal. The noise signal had its channel power measured the same way as the data signal. With these measures, it was possible to calculate the signal-to-noise ratio (SNR). With the

noise being added to the transmission line, the transmitter board was commanded to send 10000 packets of 100 octets (800 bits) to the receiver. If a sent packet was not detected by the receiver or got to the receiver with at least one wrong bit, it was considered a packet with an error and added to the Packet Error Rate. Since the goal was to trace a curve of the percentage of wrong packets, the sum of packets with an error and/or not received was divided by the total sent packets and multiplied by 100 to calculate the PER, as shown in Eq.(3.3).

The number of points in each one of the curves is not necessarily the same, since some modulations with higher data rates allowed a fast measurement of PER, while other modulations with lower data rates made the procedure too long, taking up to three days to measure all the needed points in the same conditions. So the whole procedure, starting from measuring the channel power of the transmitted signal, was repeated as many times as necessary for each modulation so its PER vs SNR curve would have a relevant amount of measured points while maintaining data quality. This curve should have the values of PER varying from 100% to 1%.

$$\text{PER} = ((\text{Packets with wrong bits} + \text{Packets not received})/(\text{Sent Packets})) \times 100 \quad (3.3)$$

During the process of calculation of the Packet Error Rate, it was desired to also collect the Bit Error Rate (BER) for the tested modulations when exposed to AWGN interference. The conducted experiment was the same described in the previous paragraphs of this section, but instead of calculating the percentage of wrong packets, the percentage of wrong bits was calculated. As 10000 packets of 100 octets (800 bits) were transmitted to the receiver, the total number of transmitted bits for each experiment was 8 million bits. So if at the end of the experiment 4 million bits were wrong, that meant a 50% or, as it will be shown in the resulting curves, 0.5 Bit Error rate. Due to technical difficulties with the Atmel AT86RF215 transceiver software at the time, it was not possible to gather the BER data for the Wi-SUN curves, so the resulting BER curves for the LoRa modulation were not compared to Wi-SUN, but rather to the LoRa curves of different parameters.

3.3 Results and Discussion

3.3.1 Sensitivity

Using the methods described in 3.2.2, the sensitivity was measured and calculated for each one of the studied modulations. Table 3.6 shows the measurement results.

Chip	Modulation	Sensitivity	Datasheet Sensitivity
Atmel AT86RF215	GFSK-Rb50-Mod.Ind.1.0	-106.37 dBm	-109 dBm
	GFSK-Rb150-Mod.Ind.0.5	-103.14 dBm	-102 dBm
	GFSK-Rb200-Mod.Ind.0.5	-102.34 dBm	-102 dBm
	OFDM-Option1-MCS0	-103.71 dBm	-109 dBm
	OFDM-Option1-MCS1	-104.81 dBm	-109 dBm
	OFDM-Option1-MCS2	-104.55 dBm	-107 dBm
	OFDM-Option1-MCS3	-102.82 dBm	-104 dBm
	OFDM-Option2-MCS4	-102.01 dBm	-104 dBm
	OFDM-Option3-MCS5	-102.02 dBm	-102 dBm
	OFDM-Option4-MCS6	-100.26 dBm	-101 dBm
	OQPSK-CR100-RM0	-117.24 dBm	-123 dBm
	OQPSK-CR2000-RM0	-108.32 dBm	-116 dBm
Semtech SX1276	LoRa-CSS-SF7-BW500	-104.33 dBm	-117 dBm
	LoRa-CSS-SF10-BW500	-114.4 dBm	-126 dBm
	LoRa-CSS-SF12-BW500	-120.61 dBm	-131 dBm
	LoRa-CSS-SF7-BW250	-111.95 dBm	-120 dBm
	LoRa-CSS-SF7-BW125	-114.97 dBm	-123 dBm
	LoRa-CSS-SF12-BW125	-128.53 dBm	-137 dBm
	LoRa-CSS-SF7-BW250-CR8	-112.95 dBm	-120 dBm

Table 3.6 – Sensitivity experiment results alongside with datasheet sensitivity values.

The sensitivity of most of the studied modulations did not reach the levels stated by the manufacturers in the datasheets. There are many probable reasons for this divergence to occur, e.g. the size of packets used for the experiment (100 octets, as described in 3.2.2), the PER or BER (Bit Error Rate) boundaries used by the manufacturers when measuring sensitivity and even poor-quality implementation of the modules can cause such values to be different from the expected.

It is important to know that the modulations that benefit from spreading spectrum tend to have a higher gain in sensitivity due to processing gain, which might increase the amount of noise they can withstand and even increase how distant the receiver and transmitter pair can be from each other, but at the cost of lower data rates.

3.3.2 Additive White Gaussian Noise Performance

For each one of the studied modulations, a curve was traced to observe the PER vs SNR ratio. The following images show these graphs and help us to analyze how each technology behaves when adding an AWGN signal to the system.

Observing the curves in Fig. 3.3, it is noticeable that different bandwidths and, consequently, different data rates result in different performance. The wider bandwidth signal shows poorer performance compared to its narrower counter-part.

For the OFDM options, as observed in Fig. 3.4, the performance is strongly

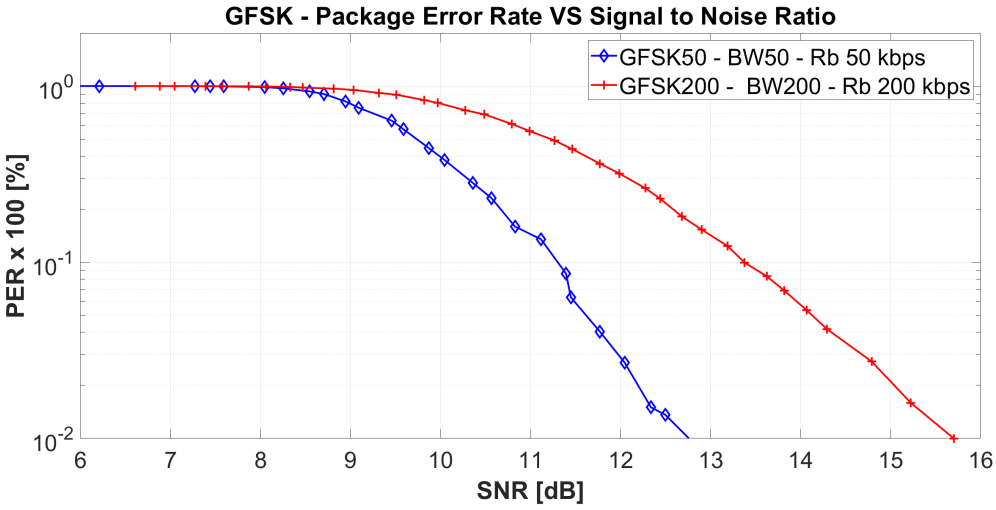

Figure 3.3 – PER vs SNR curves of the tested GFSK signals.

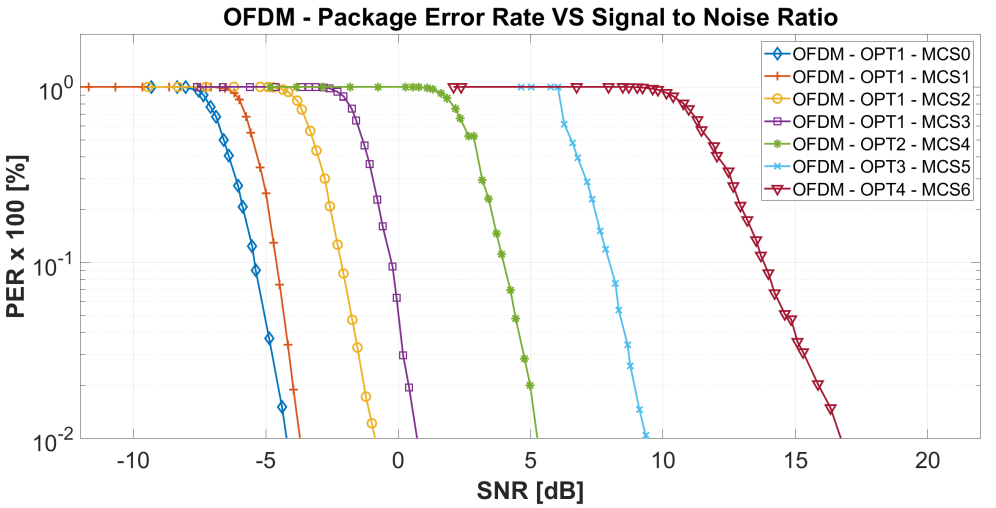

Figure 3.4 – PER vs SNR curves of the tested OFDM signals.

related to the modulation and other parameters of the carriers in each MCS (Modulation and Coding Scheme). By looking only to the curves that show Option 1 variants (which have the same bandwidth and the same number of carries, but different MCS), it is also possible to relate the robustness to the data rate of the transmitted signals, since the modulation can endure higher signal-to-noise ratios for lower data rates.

The resulting PER curves from the experiments using LoRa CSS modulation are displayed in Fig. 3.5, and show that its performance is extremely related to the spreading factor of the signal. While the bandwidth may increase or decrease robustness, for a fixed spreading factor, an increase in the spreading factor value drastically changes the amount of noise the modulation can tolerate. This also indicates a strong correlation between data rate and performance, once the more spread is the signal, the less data it can transmit for the same bandwidth and same time window.

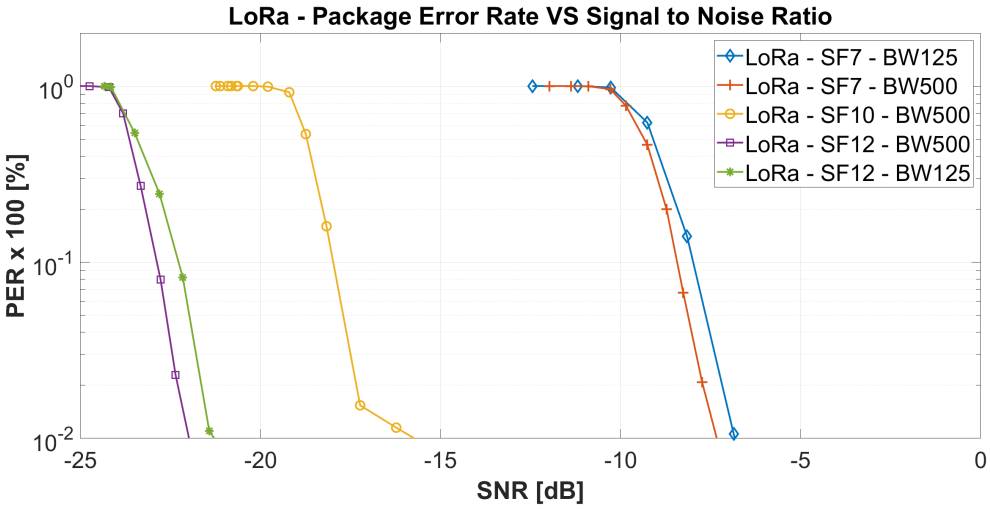

Figure 3.5 – PER vs SNR curves of the tested LoRa signals.

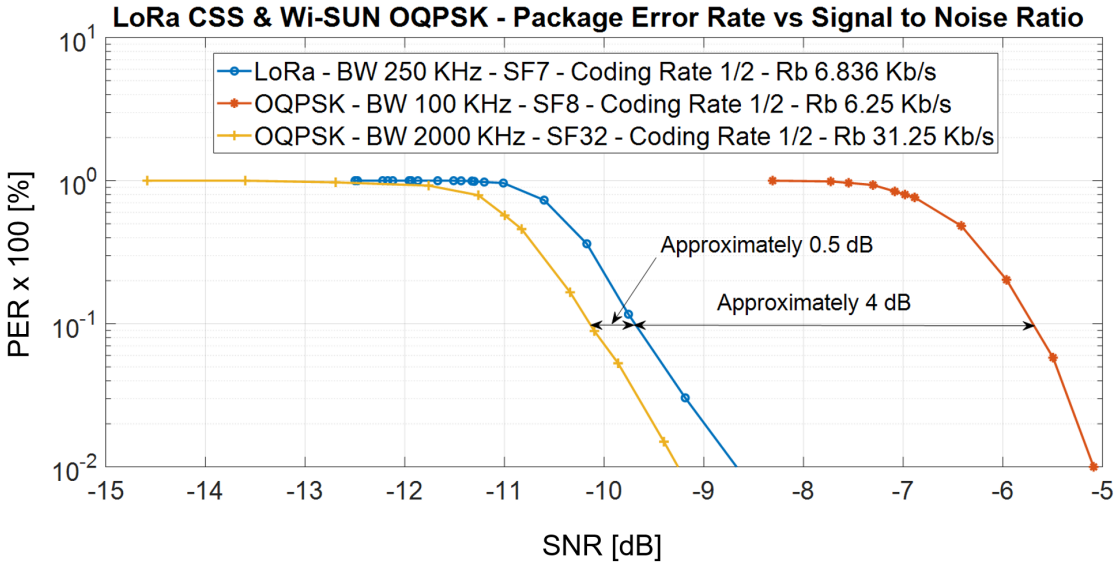

Figure 3.6 – PER vs SNR graphical comparison between LoRa CSS and O-QPSK.

Within the Atmel AT86RF215 modulation options, the ones that are straight comparable to LoRa CSS are the O-QPSK variants. The O-QPSK also benefits from spreading its signal over the bandwidth, which accomplishes better performance in detriment of the data rates, this is known as processing gain.

Observing Fig. 3.6, the OQPSK signal with narrower bandwidth (100 KHz) was the closest to the tested LoRa signal in terms of data rate within the OQPSK available modulations in the Wi-SUN chip. The OQPSK with a wider bandwidth (2000 KHz had the next closest data rate to the tested LoRa signal. This allowed for a comparison where the chosen LoRa signal would have a data rate that was higher than the first OQPSK signal and lower than the second OQPSK signal. It becomes clear that the tested LoRa signal has better performance (proportional to the difference between bandwidths) over

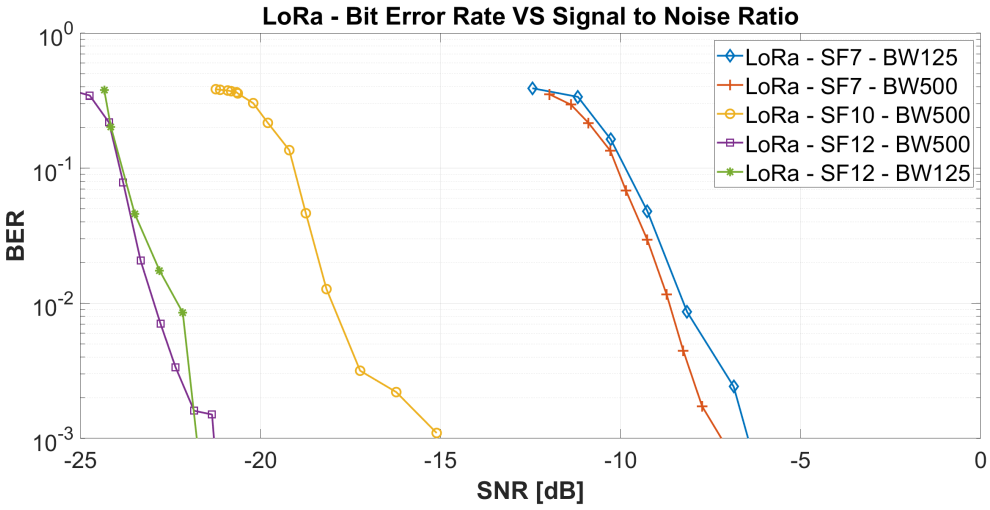

Figure 3.7 – BER vs SNR curves of the tested LoRa signals.

an O-QPSK signal with a similar data rate when exposed to additive white Gaussian noise.

3.3.3 LoRa's BER Performance Against Additive White Gaussian Noise

As it was not possible to collect BER data for the Wi-SUN modulations, the following results were not considered when comparing the technologies, but should not be completely ignored as they can be used for other purposes and even compared between themselves.

In Fig. 3.7, the Bit Error Rate curves of LoRa CSS modulation using the same coding rate, but varying spreading factor and bandwidth are displayed. It can be observed that LoRa CSS AWGN performance is extremely related to the spreading factor of the signal, as it is also seen in Fig. 3.5 in the Packet Error Rate curves. It is important to address that in Fig. 3.7, the curves with a spreading factor of 12 cross one another at some points, which might have occurred due to signal echos (multiple reads of the same signal with different gains) in the points where the noise was lowest, causing a little disturbance in the measurement.

In Fig. 3.8, the Bit Error Rate curves for two LoRa signals using two different coding rates are compared. As all the other parameters used for these signals were the same (e.g. bandwidth and spreading factor), the observed curves show that there is little performance to almost no performance gain between these LoRa signals. In Fig. 3.8, although the signal with a higher coding rate does show better performance for the most of the curve, the performance gain, in the farthest point between the curves, does not reach a difference bigger than 0.5 dB. So, as the data rates drop when using a higher coding rate, it should be considered that the gain, in this case, is little and might not be

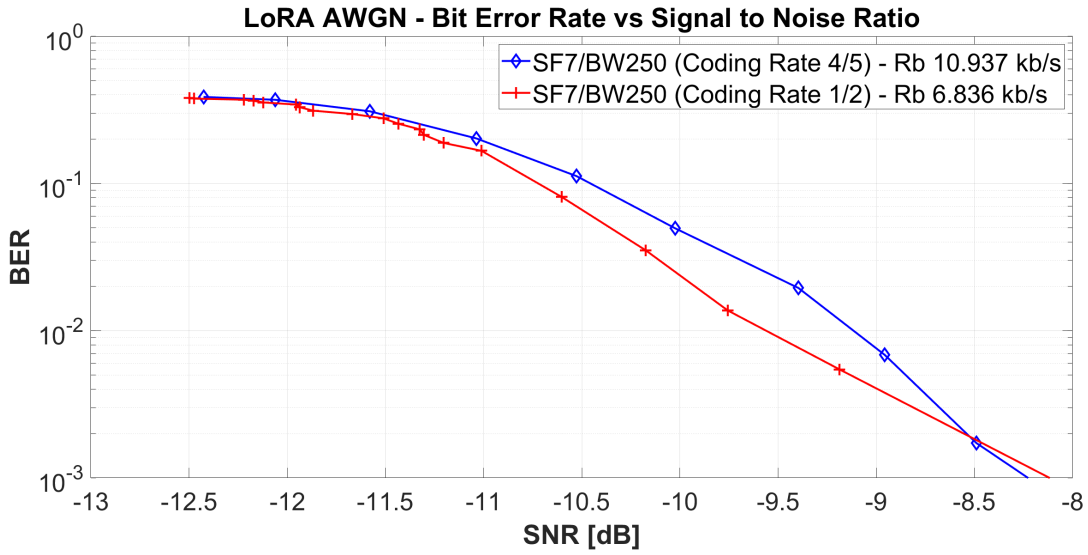

Figure 3.8 – BER vs SNR graphical comparison between LoRa using Coding Rate 4/5 and LoRa using Coding Rate 1/2 for Spreading Factor 7 and BW 250kHz.

worth the loss in data rate depending on the application where these LoRa schemes can be deployed. This result also points again towards the fact that LoRa's CSS performance is much dependable on its spreading factor rather than in other parameters as seen in Fig. 3.8, Fig. 3.7 and Fig. 3.5.

4 Multipath-Channel Performance Experiment

4.1 Introduction

In this chapter, experimental procedures for obtaining multipath fading performance of networking devices are presented alongside with methods and equipment setups, which are proposed to create a controlled testing environment, in order to achieve fair conditions for systematically compare these devices and the technologies they use.

4.1.1 Wireless Channels

For a better understanding of a modulation advantages and disadvantages, it is important to understand the basic characteristics of its performance over wireless channels. The transmitted signal is affected by the channel as it goes through the path from the transmitter to the receiver, depending on the distance between the two antennas (path loss), the path taken by the signal (shadowing), and the environment - buildings and other objects - around the path (multipath fading) [32]. These three phenomena are grouped into large-scale or small-scale propagation effects. Path loss and shadowing are referred to as large-scale since they cause signal variations over large distances, while multipath fading is classified as small-scale attenuation since the variations caused by it occur over very short distances [33]. This work focuses only on the small-scale propagation effects. The multipath fading is related to the signal reflections caused by the objects located around the path of the wireless signal. These reflections might reach the receiver with different amplitudes and phases, which may combine coherently or incoherently, thus increasing or decreasing the received power. If a single pulse is transmitted over a multipath channel, there will be multiple copies at the receiver at different times, since different paths have different lengths. Thus, the channel impulse response described as a discrete number of impulses as shown in (4.1):

$$h\left(t,\tau\right)=\sum_{i=1}^{N}\alpha_{i}\left(t\right)e^{-j\theta_{i}(t)}\delta\left(\tau-\tau_{i}\left(t\right)\right), \tag{4.1}$$

where, N stands for the number of the channel coefficients, and $\alpha_i(t)$, $\theta_i(t)$ and $\tau_i(t)$ stand for the amplitude, phase and delay spread of the *ith* multipath component. Apart from the multi-path fading models, this fading can be separated into two types due to the time dispersive nature of the channel - flat and frequency selective fading. These types of fading

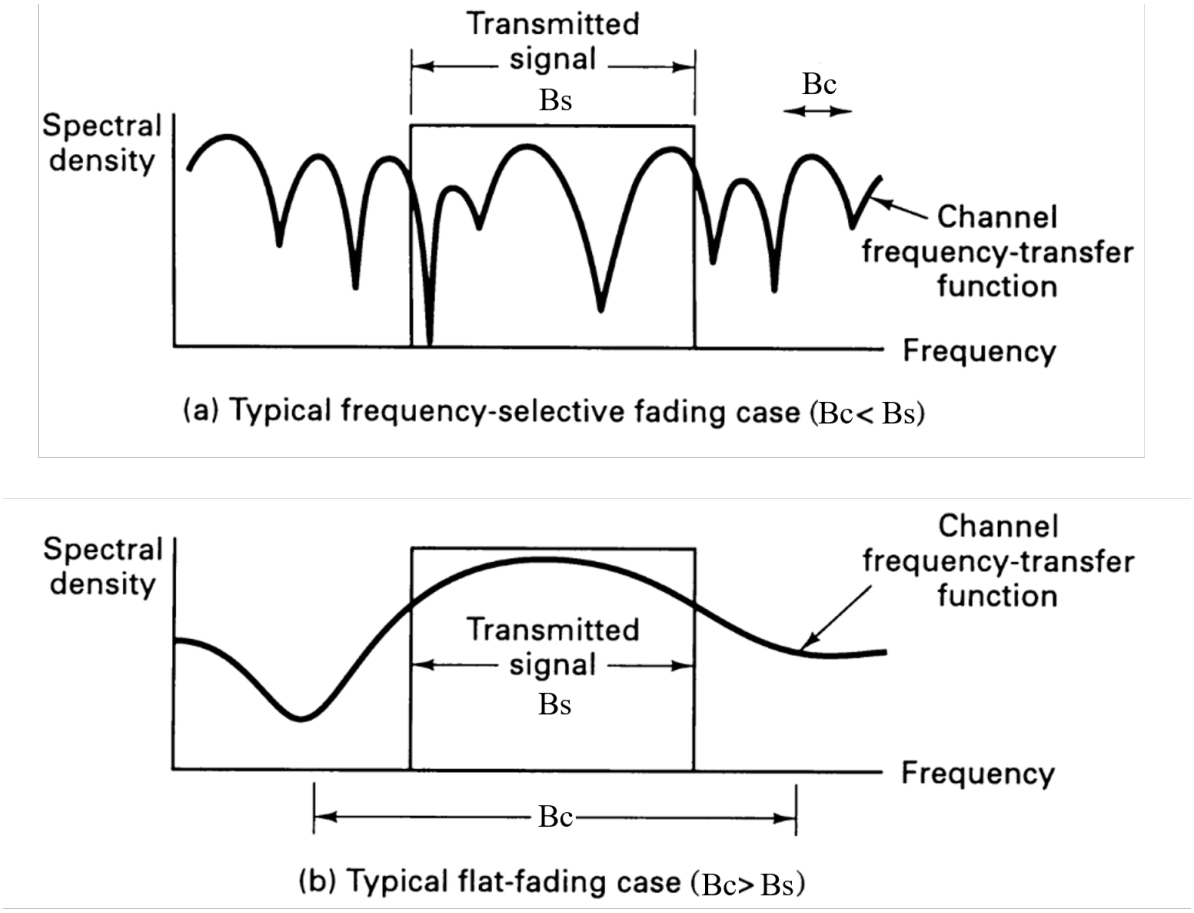

Figure 4.1 – Channel coherence bandwidth Bc and signal bandwidth Bs [4]

depend on the relation between signal and channel parameters - bandwidth, delay, and symbol period -, characterizing the channel according to its coherence bandwidth (Bc) and time delay spread ($\sigma\tau$). The Bc is the frequency bandwidth for which the channel characteristics remain similar, i.e., the channel is considered to pass all the frequency components with almost equal gain and linear phase. The Bc is inversely related to the channel time delay spread ($\sigma\tau$), which is the time interval between the arrival of the first received signal component and the last received signal component of the same transmitted single pulse. When the channel's Bc is greater than the signal's bandwidth (Bs), hence, $\sigma\tau$ is smaller than the duration of the transmitted symbol (Ts), the channel is considered flat fading. On the other hand, for a frequency selective fading, $Bs > Bc$ and $Ts < \sigma$. Both cases, flat and frequency selective fading, are depicted in Fig. 4.1.

In this work, we used four channel models to evaluate the two commercial integrated circuits for LoRa and IEEE802.15.4g. These are pre-existing channel models modeled and defined in other articles which are listed next: URBAN CHANNEL (STAR) [34], SUI-1 CHANNEL [35], SUI-5 CHANNEL [35] and finally SUI-6 CHANNEL [35].

Mode LoRa CSS	Bandwidth [kHz]	Spreading Factor	Coding Rate	Data Rate [Kbps]
SF7-BW500	500	7	4/5	21.875
SF12-BW125	125	12	4/5	0.293
SF7-BW250-CR8	250	7	1/2	6.836

Table 4.1 – LoRa Parameters.

Parameter	Option	
	1	4
Bandwidth [kHz]	1094	156
MCS0 Data Rate [Kbps]	100	N/A
MCS6 Data Rate [Kbps]	N/A	300

Table 4.2 – MR-OFDM Characteristics.

MCS	Modulation	Code Rate	Frequency Spreading
0	BPSK	1/2	4x
6	16-QAM	3/4	No Spread

Table 4.3 – Modulation and Coding Schemes for MR-OFDM.

4.1.2 Characteristics and Parameters

Tables 4.1 to 4.4 present the main parameters of LoRa and IEEE 802.15g respectively. Those parameters will be explored in the following sections, during the evaluation of the integrated circuit.

4.2 Experimental Procedures

4.2.1 Materials and Equipment

The main goal was to systematically test the modulation technologies in a controlled environment. To create such conditions, the equipment and other necessary materials are listed below:

Mode O-QPSK	CR100-RM0	CR2000-RM0
Chip Rate [kchip/sec]	100	2000
Bandwidth [kHz]	100	2000
Spreading Factor	8	32
Coding Rate	1/2	1/2
Data Rate [Kb/sec]	6.25	31.25

Table 4.4 – MR-O-QPSK Parameters.

- 02 Atmel AT86RF215 – 802.15.4g Transceiver
- 02 Semtech SX1276 – LoRa Transceiver
- 01 Laptop with MATLAB
- 01 Spectrum Analyzer – Agilent E4404B
- 01 Signal Generator – Keysight N5172B
- 01 RF Channel Emulator – TAS 4500
- 01 Shield Box
- 02 Variable Attenuators (10 dB/step and 1dB/step)
- 01 In-line Attenuator (55.34 dB)
- 02 Signal Divider and Combiner
- Miscellaneous Adapters
- Cables for the necessary connections

4.2.2 Multipath-channel Experiment

A channel is a medium where signals travel from transmitter to receiver. Each environment has a different channel with characteristics that are inherent to the elements of each place. The multipath-channel experiment uses a channel emulator that allows the observation of the behavior of each modulation in different environments. This way, it is possible to explore the performance of the target technologies towards models of channels that represent real environments where these technologies shall be deployed. To perform a multipath-channel test, the equipment and materials were set as shown in Fig. 4.2.

The first step was to configure the channel emulator with a tapped delay line model, which consists of three taps. Each tap models a delay, attenuation, and, when the channel presents mobility, a velocity related to the Doppler effect.

Next, using the transmitter board, a continuous signal was transmitted indefinitely. Using the channel emulator's auto-calibration option, the equipment was adjusted to the power of the transmitted signal. The transmission was then interrupted.

The spectrum analyzer was configured to measure the channel power of the whole bandwidth of the targeted signal, using the same center frequency as of the signal and a resolution bandwidth of 1 kHz. After the measurement, the transmission was interrupted once more. Using the signal generator, an AWGN signal was added to the

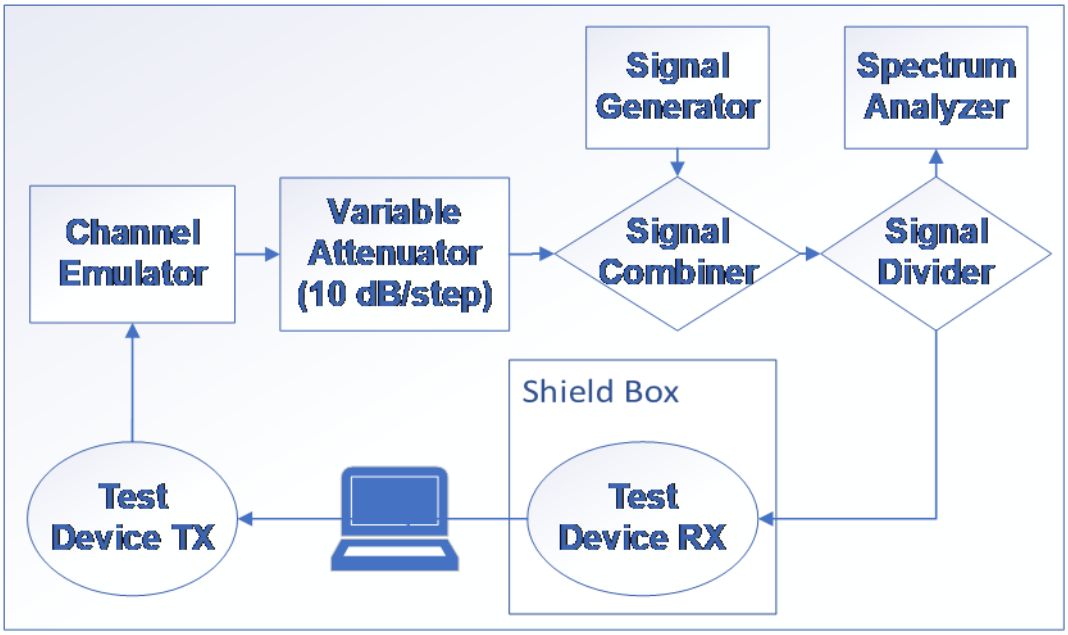

Figure 4.2 – Flow chart representing the setup necessary to measure the performance of a device under a multipath channel.

system. This signal had the same center frequency and the same bandwidth as the evaluated modulated signal. The noise signal had its channel power measured the same way the data signal was measured.

With the noise being added to the transmission line, the transmitter board was commanded to send 10000 packets of 100 octets (800 bits) to the receiver. If a sent packet was not detected by the receiver or got to the receiver with at least one wrong bit, it was considered a packet with an error and added to the Packet Error Rate. Since the goal was to trace a curve of the percentage of wrong packets, the sum of packets with an error and/or not received was divided by the total sent packets and multiplied by 100 to calculate the PER, as previously shown in Equation (3.3) in chapter 3.

The number of points in each one of the curves is not necessarily the same, since some modulations with higher data rates allowed a fast measurement of PER, while other modulations with lower data rates made the procedure too long, taking up to three days to measure all the needed points in the same conditions. So the whole procedure, starting from measuring the channel power of the transmitted signal, was repeated as many times as necessary for each modulation so its PER vs SNR curve would have a relevant amount of measured points while maintaining data quality. This curve should have the values of PER varying from 100% to 1%.

While collecting the Packet Error Rate, it was desired to also collect the Bit Error Rate (BER) for the tested modulations when exposed to AWGN interference. The conducted experiment was the same described in the previous paragraphs of this section,

	Tap 1	**Tap 2**	**Tap 3**	**Unit**
Delay	0.72	2.17	3.62	μs
Power	0	-13	-33	dB

Table 4.5 – Urban Channel (STAR).

	Tap 1	**Tap 2**	**Tap 3**	**Unit**
Delay	0	0.4	0.9	μs
Power	0	-15	-20	dB

Table 4.6 – SUI1 without Doppler Effect.

	Tap 1	**Tap 2**	**Tap 3**	**Unit**
Delay	0	4	10	μs
Power	0	-5	-10	dB

Table 4.7 – SUI5 without Doppler Effect.

but instead of calculating the percentage of wrong packets, the percentage of wrong bits was calculated. As 10000 packets of 100 octets (800 bits) were transmitted to the receiver, the total number of transmitted bits for each experiment was 8 million bits. So if at the end of the experiment 4 million bits were wrong, that meant a 50% or, as it will be shown in the resulting curves, 0.5 Bit Error rate. Due to technical difficulties with the Atmel AT86RF215 transceiver software at the time, it was not possible to gather the BER data for the Wi-SUN curves, so the resulting BER curves for the LoRa modulation were not compared to Wi-SUN, but rather to the LoRa curves of different parameters.

Four channel models were chosen to test the target technologies. These channel models should represent possible environments where the technologies might be deployed, such as urban centers, hilly locations, and even channels with a direct line of sight between transmitter and receiver. The parameters of each model are presented in tables 4.5 to 4.8 and their power delay profiles are shown in figures 4.3 to 4.6.

	Tap 1	**Tap 2**	**Tap 3**	**Unit**
Delay	0	14	20	μs
Power	0	-10	-14	dB
Doppler	0.4	0.3	0.5	Hz

Table 4.8 – SUI6.

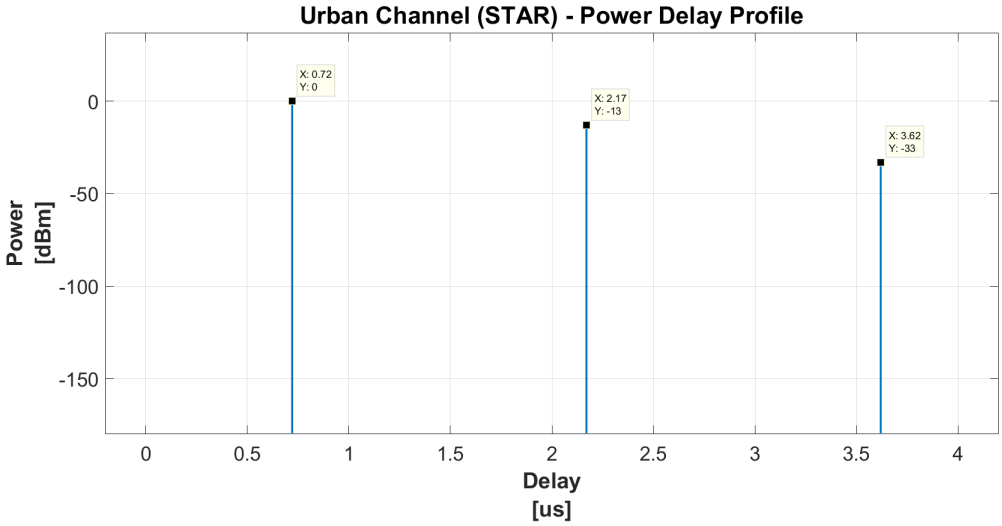

Figure 4.3 – Urban Channel (STAR) model power delay profile.

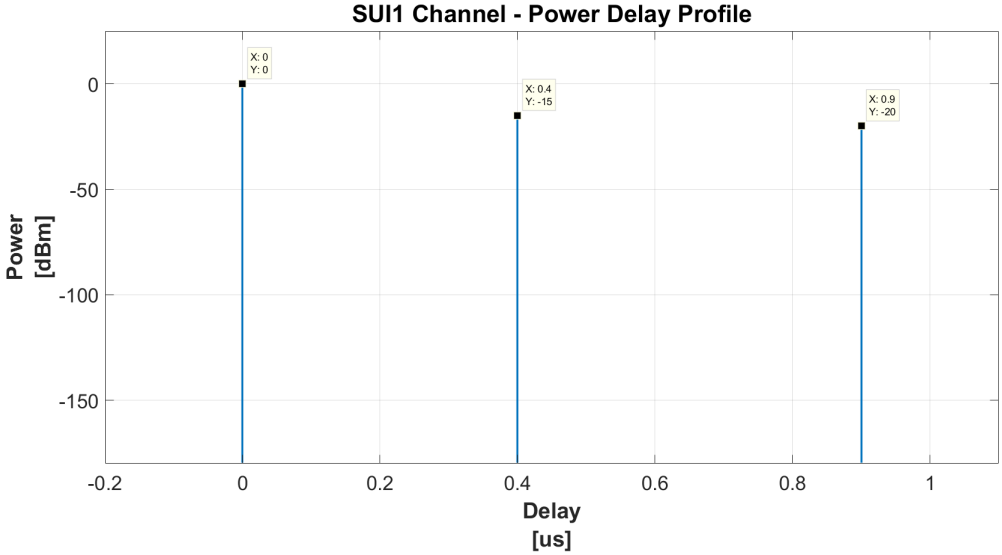

Figure 4.4 – SUI1 Channel model power delay profile.

4.3 Results and Discussion

4.3.1 STAR Channel Performance

This channel model should be a good representation of an urban area, with the following conditions: the transmitter is positioned on the top of a building, 15 meters high, while the receiver is positioned just 2.5 meters high. This is very common when the communication technology uses star topology.

Although there is a relatively low loss in performance, it is possible to observe, in Fig. 4.7, that the modulations are in fact affected by this channel model.

For this channel, the performance of the tested LoRa signals is closest to the AWGN performance when its spreading factor is highest. This happens due to the

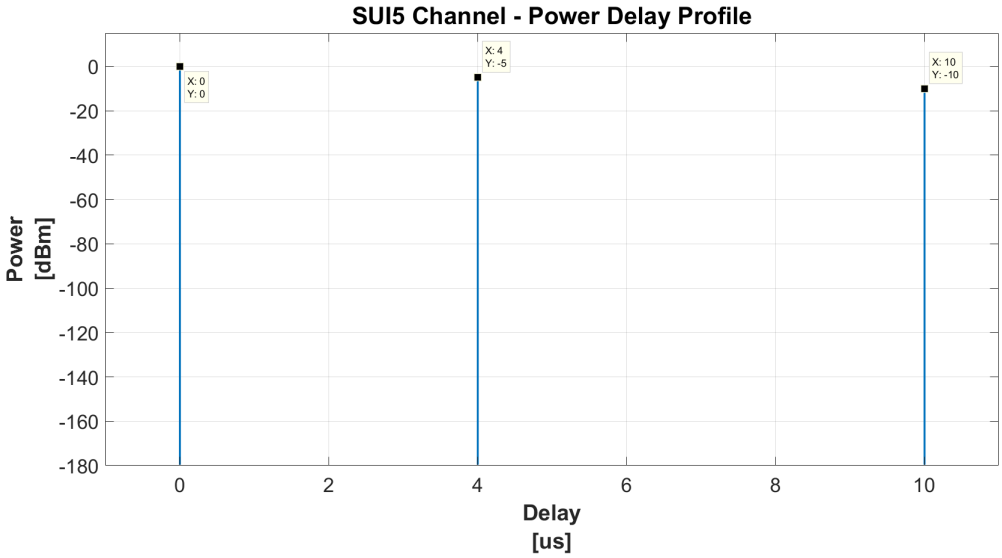

Figure 4.5 – SUI5 Channel model power delay profile.

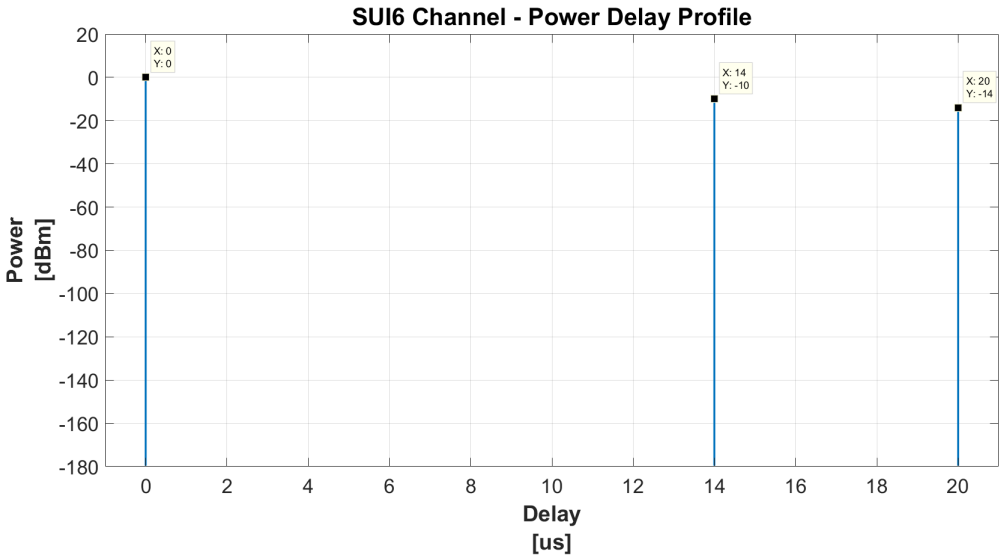

Figure 4.6 – SUI6 Channel model power delay profile.

processing gain that comes from the multiple repetitions of the signal (spreading) within the bandwidth. On the other hand, OFDM's performance curve shows a slighter more affected signal probably due to its wider bandwidth and lesser frequency spreading which, for this modulation code scheme (MCS0) is a 4x spread.

4.3.2 SUI1 (without Doppler) Channel Performance

The SUI1 channel model represents a flat terrain, with a light tree density environment and a direct line of sight between the transmitter and the receiver. This means this channel is not severe and is very close to the representation of a rural environment channel.

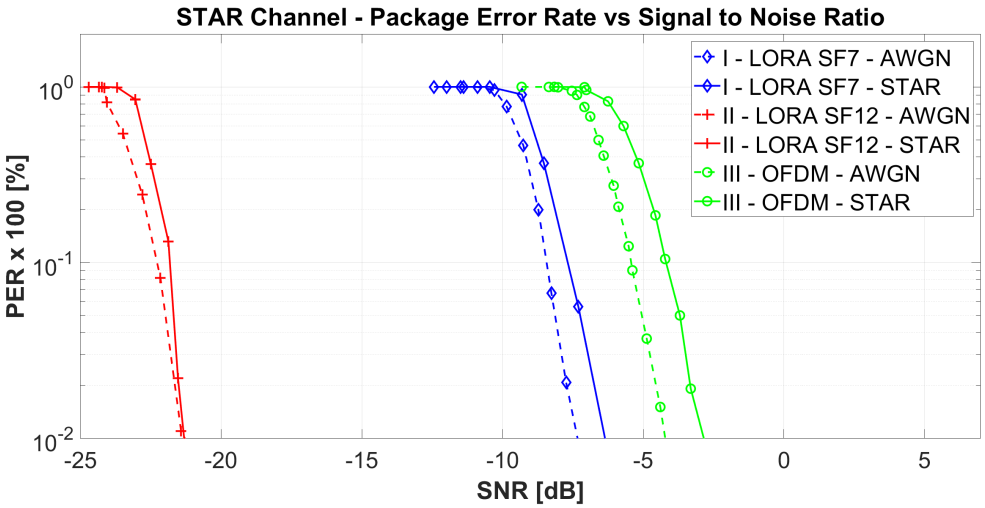

Figure 4.7 – PER vs SNR curves of the tested signals for the Urban Channel. (I-LoRa Spreading Factor 7, Bandwidth 500 kHz, Data Rate 21.875 Kb/s. II-LoRa Spreading Factor 12, Bandwidth 125 kHz, Data Rate 0.293 Kb/s. III-OFDM Option 1, MCS0, Data Rate 100 Kb/s.

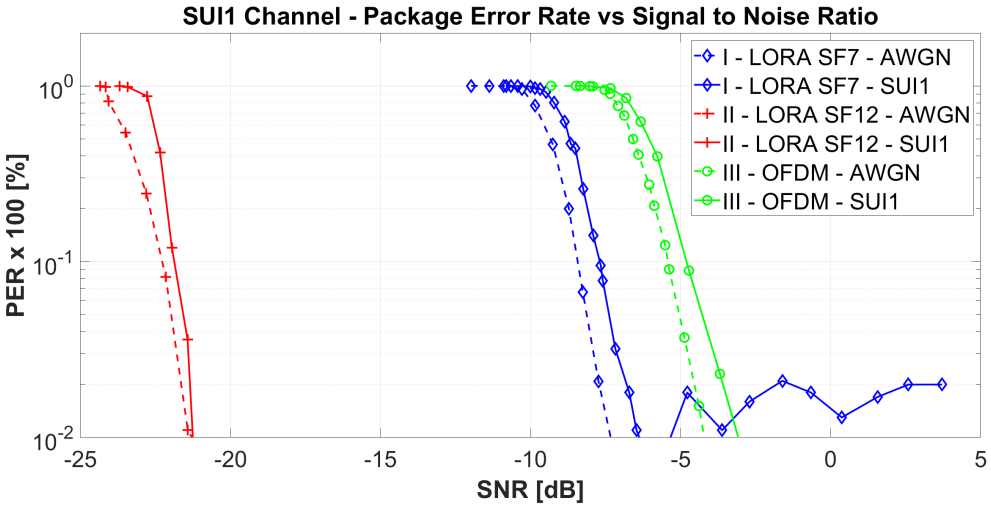

Figure 4.8 – PER vs SNR curves of the tested signals for the SUI1 Channel without Doppler. (I-LoRa Spreading Factor 7, Bandwidth 500 kHz, Data Rate 21.875 Kb/s. II-LoRa Spreading Factor 12, Bandwidth 125 kHz, Data Rate 0.293 Kb/s. III-OFDM Option 1, MCS0, Data Rate 100 Kb/s.

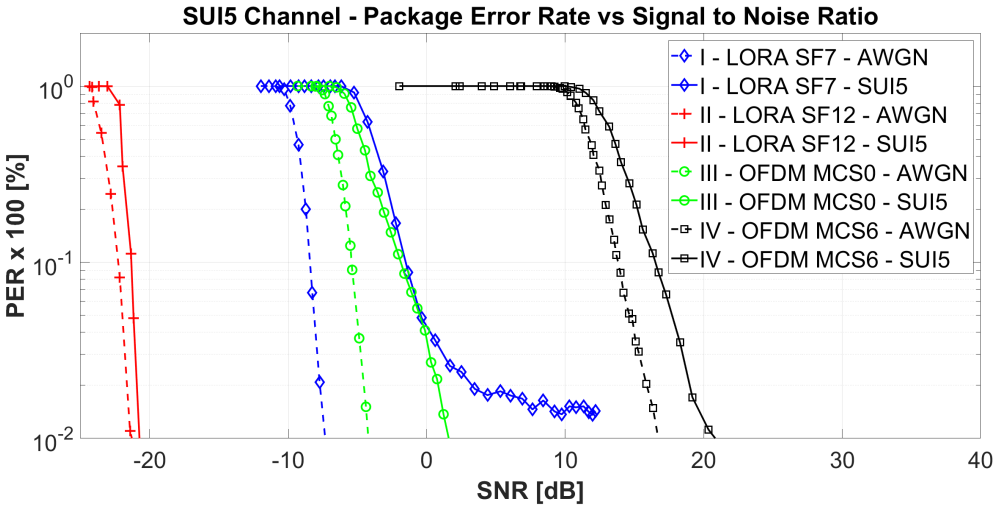

Figure 4.9 – PER vs SNR curves of the tested signals for the SUI5 Channel without Doppler. (I-LoRa Spreading Factor 7, Bandwidth 500 kHz, Data Rate 21.875 Kb/s. II-LoRa Spreading Factor 12, Bandwidth 125 kHz, Data Rate 0.293 Kb/s. III-OFDM Option 1, MCS0, Data Rate 100 Kb/s. IV-OFDM Option 4, MCS6, Data Rate 300 Kb/s).

None of the tested modulations has its performance severely affected by this channel when compared to their AWGN performances. This channel model does not impose a harsh condition on the tested signals, only damaging them slightly.

Based on the channel taps and the AWGN performance results for these modulations, the performance curves shown in Fig. 4.8 are expected except for the error spikes in curve I, which may occur because the receiver will get the same signal a few times, in different moments, with different power losses and this can lower the modulation's performance.

4.3.3 SUI5 (without Doppler) Channel Performance

The SUI5 model represents a hilly terrain with moderate-to-heavy tree density. It is a moderate channel model, that should affect the reception accordingly.

The curves in Fig. 4.9 show that the performance for LoRa Chirp Spreading Spectrum modulation is severely affected when using a lower spreading factor, while the channel poses almost no threat to a higher spreading factor.

OFDM performs well, having an acceptable degradation when under such conditions. It is important to notice that OFDM Option 1, MCS 0, performs better than LoRa using spreading factor 7 for this channel. This means that it is possible to achieve data rates almost 5 times higher with OFDM in this particular emulated environment.

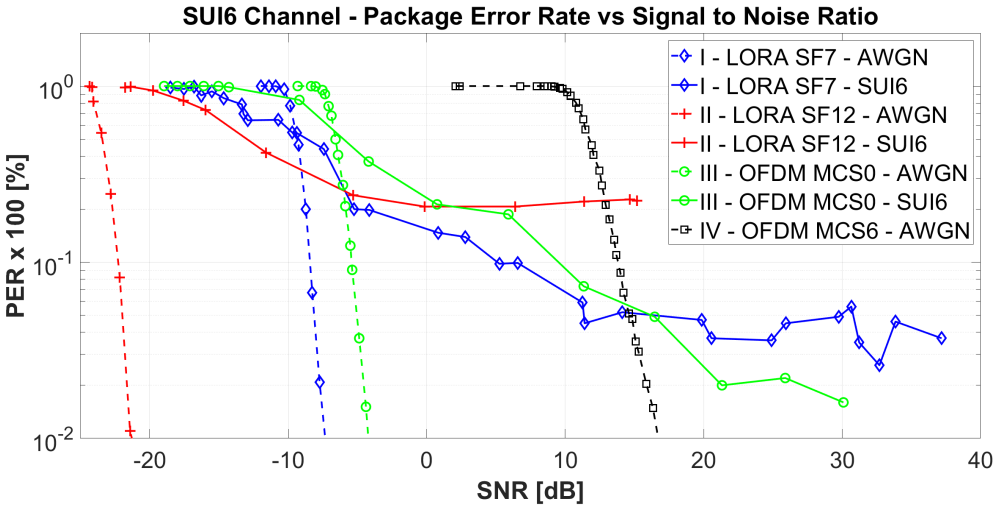

Figure 4.10 – PER vs SNR curves of the tested signals for the SUI6 Channel. (I-LoRa Spreading Factor 7, Bandwidth 500 kHz, Data Rate 21.875 Kb/s. II-LoRa Spreading Factor 12, Bandwidth 125 kHz, Data Rate 0.293 Kb/s. III-OFDM Option 1, MCS0, Data Rate 100 Kb/s. IV-OFDM Option 4, MCS6, Data Rate 300 Kb/s).

4.3.4 SUI6 Channel Performance

Although a poor performance was expected from both technologies in the presence of the SUI6 channel, the curves on Fig. 4.10 show something unexpected regarding LoRa's robustness, since the channel seems to create a "performance floor" for both LoRa curves, while the OFDM curve keeps increasing its performance for higher Signal-to-Noise ratios.

This is a major result because LoRa is supposed to be a low power technology. With the receiver not being able to read so many packets, it is possible that for a single message to be understood LoRa would have to rely heavily on transmitting the same packet several times, and this would increase power consumption greatly. Also, it is possible to achieve much higher data rates using OFDM Option 1 MCS0, which might be necessary for some applications, while having the same or better performance.

It is very important to notice that OFDM Option 4 MCS6 does not have a SUI6 performance curve, because this modulation performed very poorly in the presence of the Doppler effect, making it difficult to trace its curve in these conditions. This could also be the result of bad quality implementation of the chip, but unfortunately, it was not possible to compare its performance to the other curves given the issues encountered.

4.3.5 O-QPSK and LoRa CSS

In a more direct comparison between LoRa and 802.15.4g with similar data rates, it is possible to observe, as shown in Fig. 4.11, that O-QPSK and LoRa CSS have

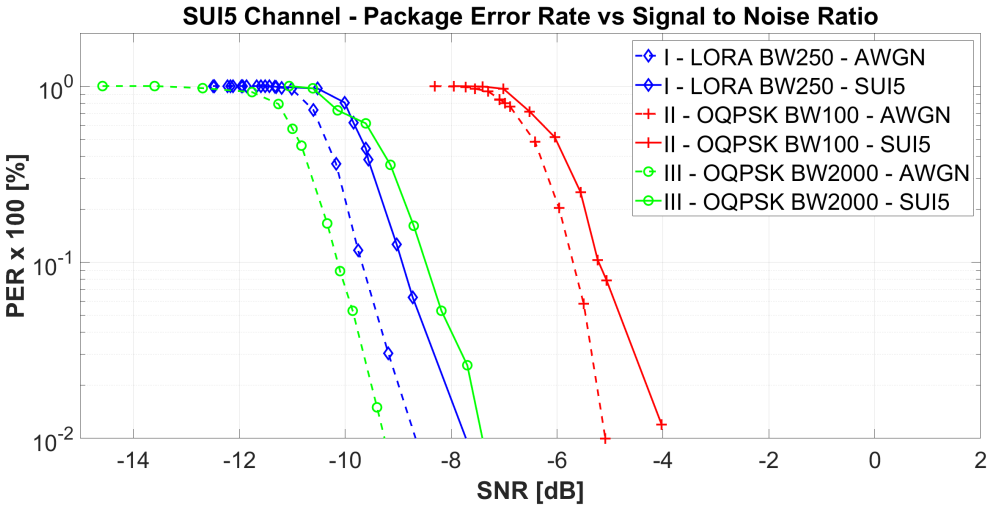

Figure 4.11 – PER vs SNR curves of the tested signals for the SUI5 Channel. (I-LoRa Spreading Factor 7, Bandwidth 250 kHz, Data Rate 6.836 Kb/s. II-O-QPSK Chirp Rate 100, Bandwidth 100 kHz, Data Rate 6.25 Kb/s. III-O-QPSK Chirp Rate 2000, Bandwidth 2000 kHz, Data Rate 31.21 Kb/s).

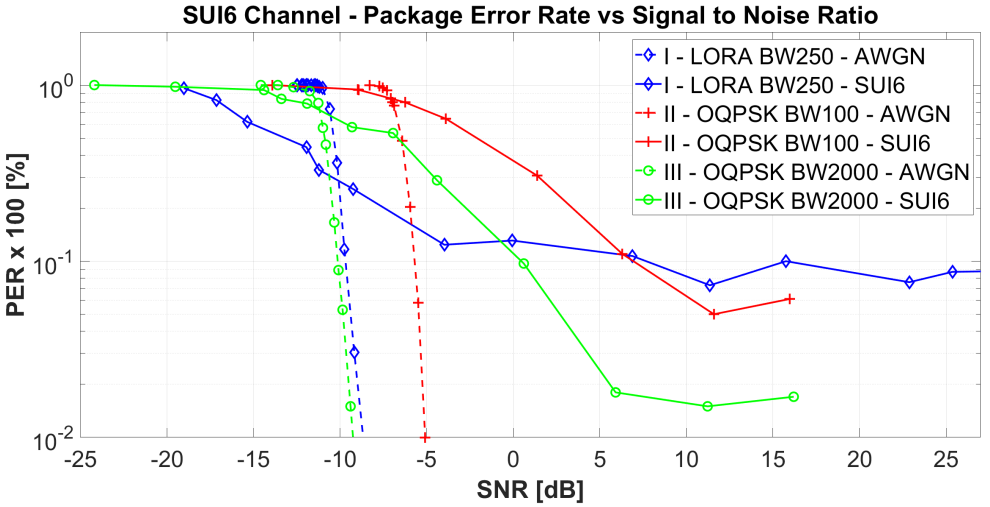

Figure 4.12 – PER vs SNR curves of the tested signals for the SUI6 Channel. (I-LoRa Spreading Factor 7, Bandwidth 250 kHz, Data Rate 6.836 Kb/s. II-O-QPSK Chirp Rate 100, Bandwidth 100 kHz, Data Rate 6.25 Kb/s. III-O-QPSK Chirp Rate 2000, Bandwidth 2000 kHz, Data Rate 31.21 Kb/s).

similar performance degradation when exposed to a moderate channel model such as the SUI5, although it is also noticeable that for the 2000 kHz O-QPSK option the performance has a greater degradation which is probably related to its wider bandwidth.

Fig. 4.12 shows a very interesting result: technologies that benefit from spreading spectrum modulations tend to perform poorly in the face of severe channels that present the Doppler Effect. This is most intriguing because spreading spectrum technologies should be resilient to Doppler. The SUI6 channel creates a performance floor for all the tested modulations, as observed in Fig. 4.12, but the two with the narrowest

bandwidths have their performance affected the most.

One hypothesis to this result is that the Doppler effect causes a frequency shift in the signals, which can cause the correlation peak to shift in time, thus lowering the correlation peak and utterly affecting synchronization.

Equation (4.2) represents a chirp signal transmitted from a moving end device.

$$s(t) = \begin{cases} A(t)\, cos\,[(\omega_0 + \omega_D)t + \frac{\mu t^2}{2}], & -T/2 < t < T/2 \\ 0, & \text{elsewhere} \end{cases} \tag{4.2}$$

where A is the amplitude of the signal, ω_0 is the angular carrier frequency, ω_D is the angular frequency shift caused by Doppler effect, t is time, μ is the chirp rate, and T is the duration of the chirp [19].

The time shift caused by the Doppler effect can be calculated as ω_D/μ. So if the chirp rate is large enough, the time shift becomes too small to be considered, but LoRa, for example, uses low chirp rates which increase the time shift, thus affecting packet reception [19].

For LoRa, the chirp rate is equal to the bandwidth [2], which means that in Fig. 4.12 the LoRa's signal chirp rate is 250 chirp/sec. So in Fig. 4.12 it is observed that the modulations with the lowest chirp rates are the most affected by the exposure to the SUI6 channel, while the modulation with the highest chirp rate is less affected by the Doppler shift. This means that these technologies are not immune to the Doppler effect and should be further tested before being deployed in mobile applications.

4.3.6 LoRa's BER Performance Against Multipath Channels

As it was not possible to collect BER data for the Wi-SUN modulations, the following results were not considered when comparing the technologies, but should not be completely ignored as they can be used for other purposes and even compared between themselves.

Although there is a relatively low loss in performance, it is possible to observe, in Fig. 4.13, that the modulations are in fact affected by this channel model.

For this channel, the performance of the investigated LoRa signals is closest to the AWGN performance when its spreading factor is the highest. This happens due to the processing gain that comes from the multiple repetitions of the signal (spreading) within the bandwidth. This result is consistent with the results observed in Fig. 4.7. Looking at the curves in Fig. 4.13, it is possible to observe that the spreading factor is the most relevant parameter for LoRa's modulation. Although bandwidth and coding rate play

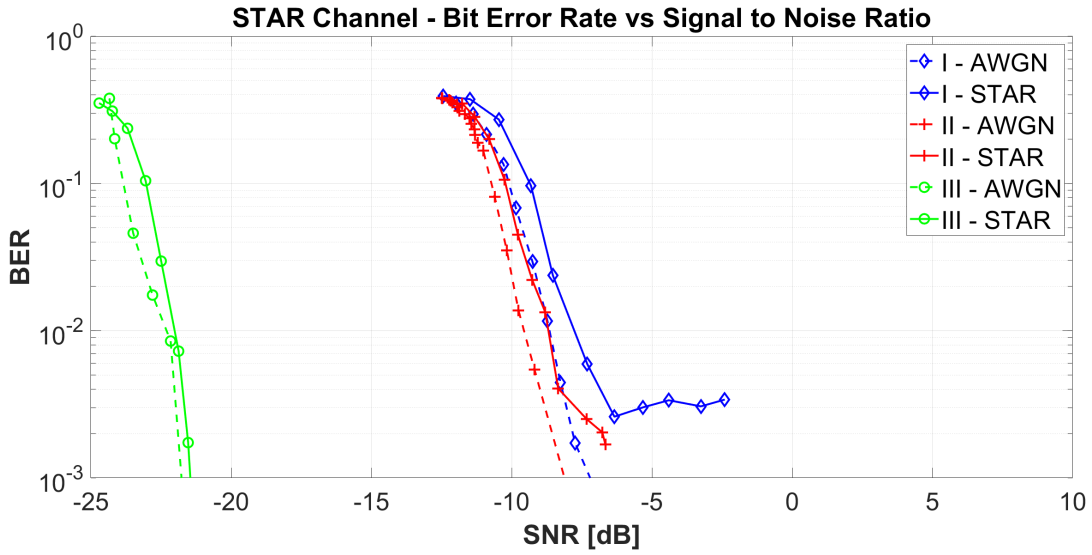

Figure 4.13 – BER vs SNR curves of the tested signals for the STAR Channel. (I-LoRa Spreading Factor 7, Bandwidth 500 kHz, Code Rate 4/5, Data Rate 21.875 Kb/s. II-LoRa Spreading Factor 7, Bandwidth 250 kHz, Code Rate 1/2, Data Rate 6.836 kb/s. III-LoRa Spreading Factor 12, Bandwidth 125 kHz, Code Rate 4/5, Data Rate 0.293 kb/s).

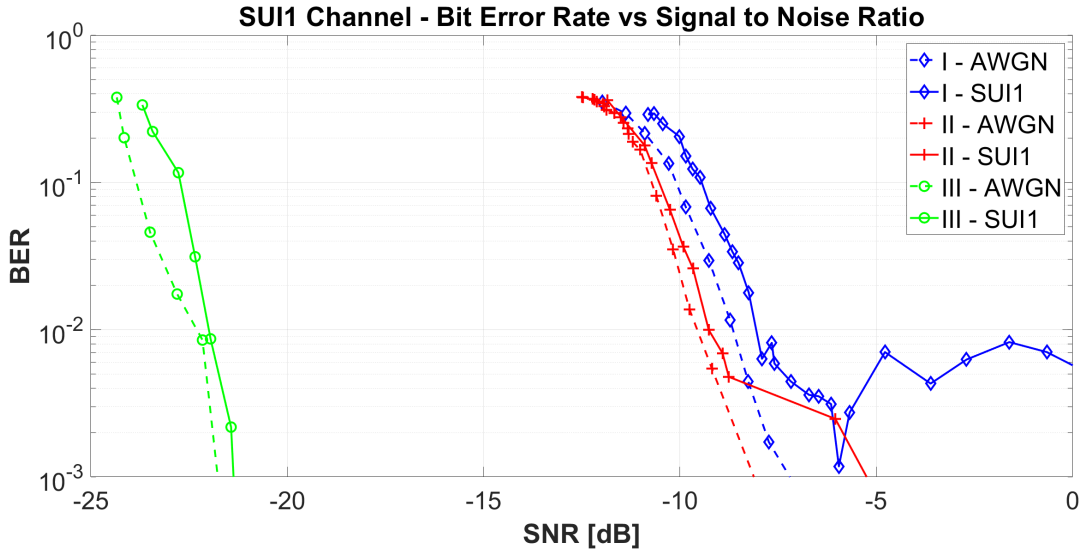

Figure 4.14 – BER vs SNR curves of the tested signals for the SUI1 Channel. (I-LoRa Spreading Factor 7, Bandwidth 500 kHz, Code Rate 4/5, Data Rate 21.875 Kb/s. II-LoRa Spreading Factor 7, Bandwidth 250 kHz, Code Rate 1/2, Data Rate 6.836 kb/s. III-LoRa Spreading Factor 12, Bandwidth 125 kHz, Code Rate 4/5, Data Rate 0.293 kb/s).

important roles in this experiment, the spreading factor is the one that determines if the modulation is more resilient to interference and channel characteristics. It should be pointed out that the modulation with the widest bandwidth starts to show a performance floor, which is important since this is a light channel model and the modulation was expected to present a better performance than the one shown in Fig. 4.13.

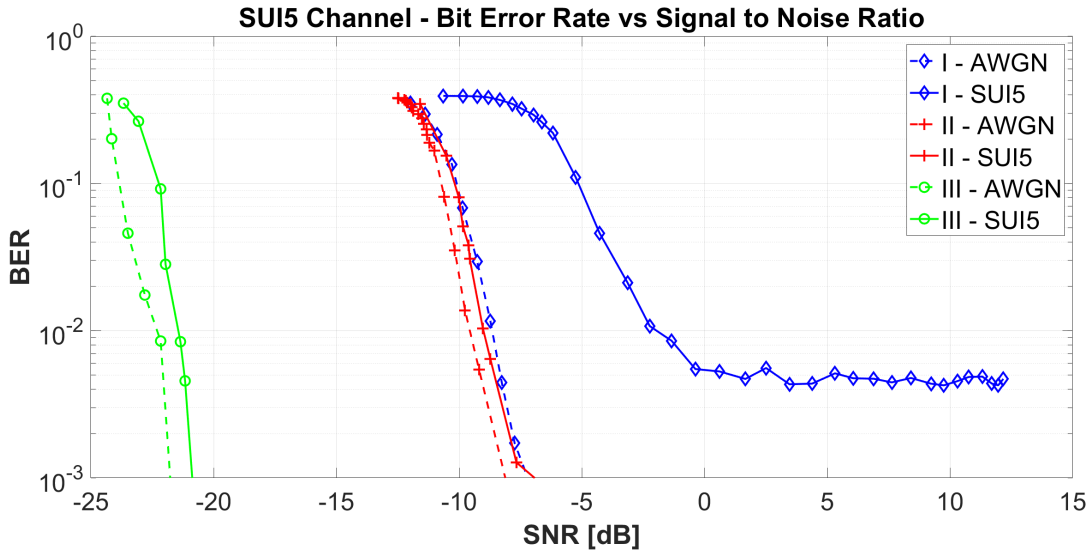

Figure 4.15 – BER vs SNR curves of the tested signals for the SUI5 Channel. (I-LoRa Spreading Factor 7, Bandwidth 500 kHz, Code Rate 4/5, Data Rate 21.875 Kb/s. II-LoRa Spreading Factor 7, Bandwidth 250 kHz, Code Rate 1/2, Data Rate 6.836 kb/s. III-LoRa Spreading Factor 12, Bandwidth 125 kHz, Code Rate 4/5, Data Rate 0.293 kb/s).

The results in Fig. 4.14 are similar to the ones in Fig. 4.13. The spreading factor makes a big difference in the modulation's performance. But Fig. 4.14 also shows that, for the LoRa's configuration with the lowest spreading factor and widest bandwidth, there is a Bit Error Rate floor. This is an interesting result and was previously observed in Fig. 4.13 and Fig. 4.8. Since the channel model does not have a Doppler variable, this result may occur because the receiver will get the same signal a few times, in different moments, with different power losses and this can lower the modulation's performance.

In Fig. 4.15, it is possible to notice that not only a higher spreading factor contributes to increasing the modulation's performance, but the bandwidth plays a big role as well. The LoRa modulation with the widest bandwidth in Fig. 4.15 is the one most affected by the SUI5 channel. In this channel model, there is no Doppler component, so the performance loss is caused only by attenuation of the signal and copies of the signal that will be received at different times. It is clear that the modulation with the widest bandwidth suffers the most because its curve for the SUI5 channel model becomes very distant from its performance curve against the Additive White Gaussian Noise, and a performance floor is also clearly observed, meaning that this modulation will not reach perfect levels of bit error rate while deployed on an environment with similar characteristics to the SUI5 channel model.

Fig. 4.16 shows interesting results as seen previously seen in Fig. 4.12. The Doppler effect component of the SUI6 channel model clearly deteriorates the performance of the system and creates a performance floor for all of them. One hypothesis to this

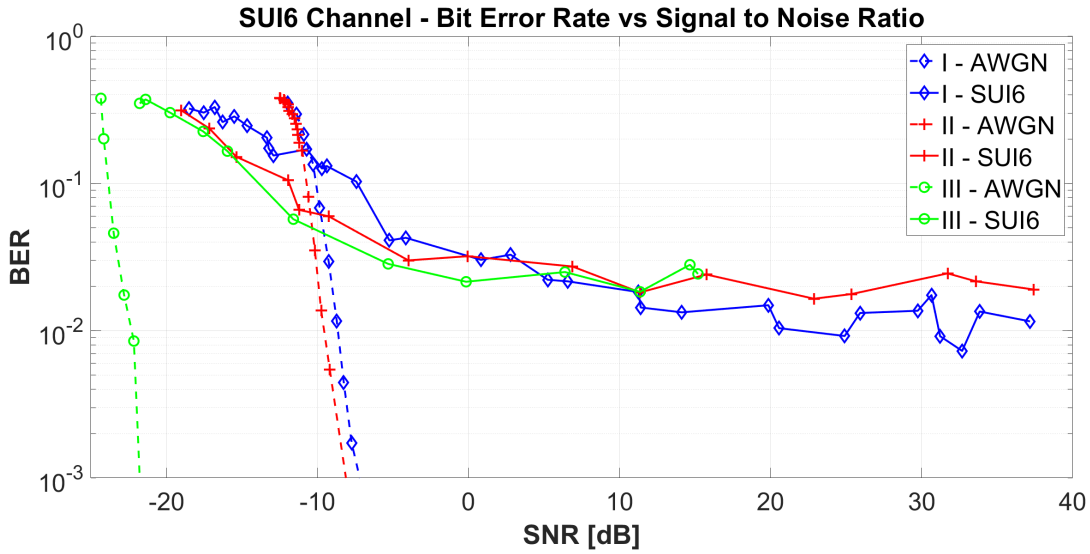

Figure 4.16 – BER vs SNR curves of the tested signals for the SUI6 Channel. (I-LoRa Spreading Factor 7, Bandwidth 500 kHz, Code Rate 4/5, Data Rate 21.875 Kb/s. II-LoRa Spreading Factor 7, Bandwidth 250 kHz, Code Rate 1/2, Data Rate 6.836 kb/s. III-LoRa Spreading Factor 12, Bandwidth 125 kHz, Code Rate 4/5, Data Rate 0.293 kb/s).

result is that the Doppler effect causes a frequency shift in the signals, which can cause the correlation peak to shift in time, thus decreasing the correlation peak and utterly affecting synchronization, as discussed in Section 4.3.4.

Since there are three LoRa curves being shown in Fig. 4.16, and based on the discussion about the Doppler Shift in Section 4.3.4, it is possible to assume that LoRa's Chirp Rate (which is equal to the size of the bandwidth) is too low to perform well against the Doppler effect, as all the curves have a very similar performance while facing the SUI6 channel model. It is interesting to notice that the three curves have different bandwidths, one of them has a higher coding rate and the other has a higher spreading factor and, even so, they behave very similarly in this experiment. Not only the multipath channel disturbs the behavior of the modulations, but the Doppler effect also utterly decreases their performance. So if LoRa is to be considered in mobile applications, it should be further investigated before full deployment, since it does not seem to be resilient to the Doppler shift.

5 Conclusions

In this dissertation, we presented a set of experiments and results which address sensitivity, additive white Gaussian noise, multipath fading, and how they affect signals transmitted by network devices. This study offers a clear observation of the performance of both LoRa and 802.15.4g technologies, providing practical information on their robustness towards noise interference and multipath fading. In the following, the main conclusions of chapters 3 and 4 are summarized.

- Chapter 3 presented a measurement setup and methods for investing both sensitivity and performance against the additive white Gaussian noise of a digital communications device systematically. Both the setup and methods can be reproduced to investigate other technologies and compare them fairly, allowing researchers and developers to choose between those technologies based on real measured data. Chapter 3 also brings results that show that LoRa Chirp Spread Spectrum modulation is a very robust option when the system is under the effect of the additive white Gaussian noise. Wi-SUN also provides very robust options with higher data rates. In direct comparison, LoRa shows better performance while benefiting from a wider bandwidth. On the other hand, the wider bandwidth may also be a problem due to the frequency band control provided by regulatory organizations. Another important point that must be looked upon is the documentation of both technologies. Wi-SUN is well documented, being standardized by the IEEE 802.15.4g standard. LoRa documentation, even with the support of LoRa Alliance, still needs work, since it is hard to find all the information one might need, and for being a proprietary spread spectrum modulation, it is difficult to find open information about it.

- Chapter 4 presented a setup and method for investigating the performance of digital communication devices under emulated multipath channels. The emulated channels are an approximation of real-world multipath channels, and this experiment should help to understand how such communication devices would behave in an environment with the same characteristics. Chapter 4 brings results that allow us to understand that when LoRa CSS modulation is under multipath channels, the technology lacks the robustness to perform well under conditions other than LOS. The results suggest that LoRa should be considered mostly for rural environments where its performance can benefit from its modulation, processing gain, and low energy consumption. The same considerations can be observed for the O-QPSK modulation, present on 802.15.4g specification. Both LoRa and O-QPSK are greatly affected by

the Doppler shift which brings their performance to a poor level when the modulations use low chirp rates, this should be considered and further analyzed if these modulations are to be used in mobile applications or deployed in conditions that involve the Doppler effect. OFDM modulation and coding schemes provide higher data rates and are less affected by NLOS channels. This makes OFDM a good candidate for deployment in smart-cities projects and other every-day urban IoT applications such as smart metering.

5.1 Future Works

Next, we highlight some ideas for future research that can yield very promising results.

- Investigating other communication technologies to increase the size of the database to allow systematic comparison between them.
- Multipath fading experiments with channels of different characteristics to help the understanding of how such channels may affect smart-cities and smart-farms.
- Signal superposition experiments are required to understand how these technologies would behave when deployed in environments that have other signals being transmitted, such as Wi-Fi and other everyday-signals.
- On-field experiments that would contribute to increase data accuracy and validate the results gathered throughout this work.

5.2 Acknowledgement

This work was supported by RD ANELL - PROJECT COPEL 2866-0366/2013 and by the Eldorado Research Institute. The author also gratefully acknowledges the Campinas State University.

Bibliography

[1] LoRa Alliance. LoRaWAN 101 - A Technical Introduction, Apr 2018. Quoted 5 times on pages 9, 12, 31, 34, and 35.

[2] Augustin, A. Yi, J Clausen, T Townsley, W. M. A Study of LoRa: Long Range Low Power Networks for the Internet of Things. *Sensors (Basel)*, 16(09)(1466), Sep 2016. Quoted 6 times on pages 9, 22, 31, 33, 34, and 64.

[3] IEEE. "IEEE Std. 802.15.4g-2012: Part 15.4: Wireless Medium Access Control and Physical Layer Specifications for Low-Rate Wireless Personal Area Networks Amendment 4: Physical Layer Specifications for Low Data Rate Wireless Smart Metering Utility Networks", 2012. Quoted 4 times on pages 9, 21, 38, and 39.

[4] Bernard Sklar. The Characterization of Fading Channels, 2002. Quoted 2 times on pages 9 and 53.

[5] www.electronics-notes.com. IEEE 802.15.4 Standard: a tutorial / primer, -. Quoted 2 times on pages 12 and 37.

[6] Semtech. Semtech - LoRa homepage, 2018. Quoted on page 21.

[7] Wi-SUN Alliance homepage, author = Wi-SUN Alliance, year = 2018, url = https://www.wi-sun.org/, urldate = 2018-11. Quoted on page 21.

[8] Sigfox S.A. Sigfox homepage, 2018. Quoted on page 21.

[9] Ingenu Inc. Ingenu RPMA, 2018. Quoted on page 21.

[10] Weightless SIG. Wightless homepage, 2018. Quoted on page 21.

[11] IoT ONE. IoT One - DASH7 homepage, 2018. Quoted on page 21.

[12] Ingenu Inc. Ingenu homepage, 2018. Quoted on page 21.

[13] Huawei Technologies Co. "NB-IoT - Enabling New Business Opportunities", 2017. Quoted on page 21.

[14] IEEE. "IEEE Std. 802.15.4-2011: Standard for Low-Rate Wireless Network", 2011. Quoted on page 21.

[15] Muñoz, J. Chang, T. Vilajosana, X. Watteyne, T. Evaluation of IEEE802.15.4g for Environmental Observations. *Sensors (Basel)*, 18(10)(3468), Oct 2018. Quoted on page 22.

[16] Harada, H. et al. IEEE 802.15.4g Based Wi-SUN Communication Systems. *Special Section on Smart Radio and Its Applications in Conjunction with Main Topics of SmartCom*, E100-B(7):1032–1043, Jul 2017. Quoted 2 times on pages 23 and 36.

[17] Christos Bouras Vasileios Kokkinos Nikolaos Papachristos. Performance evaluation of LoraWan physical layer integration on IoT devices, 2018. Quoted on page 24.

[18] Pere Tuset-Peiro Francisco Vazquez-Gallego Jonathan Muñoz Thomas Watteyne Jesus Alonso-Zarate Xavier Vilajosana. Experimental Interference Robustness Evaluation of IEEE 802.15.4-2015 OQPSK-DSSS and SUN-OFDM Physical Layers, May 2019. Quoted on page 25.

[19] Juha Petäjäjärvi Konstantin Mikhaylov Marko Pettissalo Janne Janhunen Jari Iinatti. Performance of a low-power wide-area network based on LoRa technology: Doppler robustness, scalability, and coverage, Mar 2017. Quoted 2 times on pages 25 and 64.

[20] Hendrik Linka Karl Jonas Michael Rademacher Osianoh Glenn Aliu. Path Loss Models for Low-Power Wide-Area Networks: Experimental Results using LoRa, May 2018. Quoted on page 26.

[21] Nuttakit Vatcharatiansakul Panwit Tuwanut Chotipat Pornavalai. Experimental Performance Evaluation of LoRaWAN: A Case Study in Bangkok, July 2017. Quoted on page 26.

[22] Morgan, J. A Simple Explanation Of 'The Internet Of Things', 2014. Quoted on page 30.

[23] Semtech. *AN1200.22 - LoRa Modulation Basics*. Semtech Corporation, May 2015. Quoted 3 times on pages 31, 32, and 33.

[24] LoRa Alliance. About LoRa Alliance, 2020. Quoted on page 34.

[25] Shridhar, VS. Das, A. Stevenson, I. LoRa gets a boost from the developing world, 2018. Quoted on page 36.

[26] Everynet. Everynet and American Tower Brazilian LoRa network, Jan 2020. Quoted on page 36.

[27] Business Wire. Semtech Supports Deployment of Brazilian LoRaWAN-based Network, Dec 2018. Quoted on page 36.

[28] Business Wire. LoRa Market Dynamics Report 2017: By 2022, Private Lora Networks Will Make Up Two-Thirds of the Market - Research and Markets, Oct 2017. Quoted on page 36.

[29] Wi-SUN Alliance. Member Companies Page, 2011. Quoted on page 37.

[30] IoT ONE. Wi-SUN Alliance, 2019. Quoted on page 37.

[31] Blackman, J. All about Wi-SUN, and the quiet buzz around the 'world's widest' IoT network, Oct 2018. Quoted on page 40.

[32] JAIN, R. Channel models: A tutorial. *WiMAX Forum AATG.*, pages 1–6, 2017. Quoted on page 52.

[33] Goldsmith, A. *Wireless Communications*. Cambridge University Press, 2005. Quoted on page 52.

[34] Deruyck, M. Tanghe, E. Joseph, W. Pareit, D. Moerman, I. Martens, L. Performance Analysis of WiMAX for Mobile Applications. *Wireless Communications and Networking Conference (WCNC)*, 2010. Quoted on page 53.

[35] Hart, M. et al. *Multi-hop Relay System Evaluation Methodology (Channel Model and Performance Metric*. IEEE 802.16 Broadband Wireless Access Working Group, Fev 2017. Quoted on page 53.